

Autonomous Bioisosteric Replacement for Multi-Property Optimization in Drug Design

Hyeongwoo Kim^{1†}, Seokhyun Moon^{1†}, Wonho Zhung¹,
Shinwoo Kim¹, Jaechang Lim², Woo Youn Kim^{1,2,3*}

¹Department of Chemistry, KAIST, 291 Daehak-ro, Yuseong-gu, 34141, Daejeon, Republic of Korea.

²HITS Inc., 124 Teheran-ro, Gangnam-gu, 06234, Seoul, Republic of Korea.

³Graduate School of Data Science, KAIST, 291 Daehak-ro, Yuseong-gu, 34141, Daejeon, Republic of Korea.

*Corresponding author(s). E-mail(s): wooyoun@kaist.ac.kr;

†These authors contributed equally to this work.

Abstract

Optimizing molecular properties while preserving biological activity is a central challenge in drug design. Bioisosteric replacement, which substitutes a molecular fragment with a chemically or biologically analogous moiety, offers a powerful strategy for fine-tuning properties without disrupting target binding. However, existing *in silico* approaches often rely on expert-defined modification sites or suffer from modulating multiple molecular properties simultaneously. Here, we present DeepBioisostere, a deep generative model that performs end-to-end bioisosteric replacement by autonomously selecting and substituting molecular fragments to satisfy multiple target properties. The model captures complex relationships across the molecular graph, enabling the optimization of sophisticated properties such as drug-likeness and synthetic accessibility. By learning from experimental bio-assay data, DeepBioisostere proposes replacements that maintain biological activities, even generating potential bioisosteres beyond the training data. We demonstrate the effectiveness of the model in computational hit-to-lead optimization scenarios, highlighting its potential to accelerate rational molecular design without relying on expert heuristics or pre-established substitution rules.

1 Introduction

Optimizing molecules to fulfill multiple properties such as bioactivity, biocompatibility, and synthetic accessibility simultaneously is a fundamental yet challenging goal in drug design, often requiring substantial time and cost to advance a compound from the laboratory to the clinic.[1] Given the complexity of the multi-objective design problem, a widely adopted approach is to begin with a molecule that exhibits known bioactivity toward a target protein and gradually modify its structure to enhance desirable properties. In particular, bioisosteric replacement, the substitution of one chemical moiety with another that preserves biological activity, offers a principled way to fine-tune molecular properties with minimal disruption to the molecule’s overall function.[2–4] This approach allows for delicate enhancement of specific molecular properties while maintaining the essential characteristics of the original compound, requiring careful consideration of both structural and biochemical analogies. To systematize this process, many chemists have attempted to formalize common patterns observed in successful molecular replacement, namely bioisosteres. In recent decades, numerous bioisosteres have been reported, facilitating more rational and effective chemical modifications in drug development.[5–7]

Traditional bioisosteric replacements have heavily relied on the intuition and experience of medicinal chemists.[8–11] The identification of proper bioisosteric replacements has required extensive trial and error, leading to the rise of in silico approaches.[12, 13] There have been two mainstream in silico approaches to finding bioisosteres: similarity-based and database-mining methods. Similarity-based approaches operate on the assumption that structural analogs would exhibit similar biological or chemical properties.[14] They prioritize potential bioisosteres by comparing their structural, steric, or electronic features to those of the original moiety of interest.[15–18] Diverse molecular descriptors such as fingerprints[19, 20] or structural alignments[21] were often employed to assess the similarity between chemical moieties. The similarity-based methods facilitated changes in biochemical properties during a particular chemical modification prior to experimental validation.

On the other hand, database-mining approaches identify potential bioisosteres by extraction from large chemical databases.[22–24] (See Fig. 1) They systematically enumerate pairs of molecules with only a minor structural difference, the so-called matched molecular pairs (MMPs),[25] from a large bio-assay database provided in public libraries such as ChEMBL.[26] Then, molecular fragments corresponding to the difference in each MMP are paired and identified as potential bioisosteric replacements along with their occurrences in the parent library. The differences in chemical properties and bioactivity in biochemical assays are used to predict the effect of each bioisosteric replacement, referred to as matched molecular pairs analysis (MMPA), which is essential for subsequent bioisostere recommendations. This statistical evidence enables the identification of a new bioisosteric replacement, even if the involved moieties are structurally unrelated at first glance.

Despite their advantages, existing approaches face limitations that hinder the identification of suitable chemical modifications. Similarity-based methods rely heavily on predefined molecular descriptors correlated with specific properties, making

them dependent on expert intuition and prone to arbitrariness.[27] They also struggle to identify bioisosteres that are structurally dissimilar but functionally equivalent. Meanwhile, database-mining methods are constrained by the statistical absence of uncommon or unexplored moiety pairs within the database and thus can barely identify them. Because such methods evaluate property changes based only on the exchanged fragments, they struggle to capture complex attributes such as synthesizability or drug-likeness, which inherently depend on the entire molecular context rather than local substitutions. Moreover, both approaches require the manual selection of the molecular fragment to be modified, which limits fully automated molecular optimization through bioisosteric replacement.

Recently, deep generative modeling has emerged as a powerful approach for chemical modification, capturing data-intrinsic patterns that reflect both chemical structure and biological context without relying on handcrafted descriptors.[28–41] For example, Ertl [28] and Shan and Ji [29] applied neural networks to fragment-level data derived from ChEMBL, demonstrating the ability to identify potential bioisosteric replacements beyond the training set. Jin et al. [30], Fu et al. [31], and Loeffler et al. [32] employed standard optimization algorithms to refine molecular structures toward specific biological targets with low-cost labels, such as docking scores. Zheng et al. [39] and Hu et al. [40] demonstrated that deep learning methods can be effectively applied to scaffold hopping, generating alternative scaffolds while maintaining biological activity. While the methods mark significant progress, no existing deep learning framework for chemical modification can simultaneously control multiple properties while maintaining the original bioactivity in a general manner. Addressing this gap is essential for fully leveraging bioisosteric replacement in automated, property-driven molecular design.

Here, we propose DeepBioisostere, a deep generative model for autonomous bioisosteric replacement with fine control over multiple molecular properties in an end-to-end manner, selecting modification sites and generating context-aware substitution. (See Fig. 1) We systematically curated a standardized dataset for training with experimental bioassay data to implicitly incorporate the statistical patterns of structure-activity relationships, guiding our model’s proposed replacements toward maintaining the target activity. DeepBioisostere can address the compatibility of replacement with the whole molecular structure, which is necessary to optimize delicate molecular properties such as synthetic accessibility and drug-likeness. Furthermore, we demonstrate the ability of our model to identify unexplored bioisosteric replacements that achieve the target property, which is beyond the capacity of conventional approaches. Finally, we apply DeepBioisostere in an *in silico* hit-to-lead workflow and demonstrate its ability to improve key biochemical properties of hit candidate molecules while maintaining binding affinity, offering a new opportunity toward automated drug design.

2 Results

2.1 Brief Introduction of DeepBioisostere

In this work, we regard chemical modification based on bioisosterism as a sequential process comprising three essential steps: (1) removal fragment selection, (2) insertion

Optimization of molecule via bioisosteric replacement

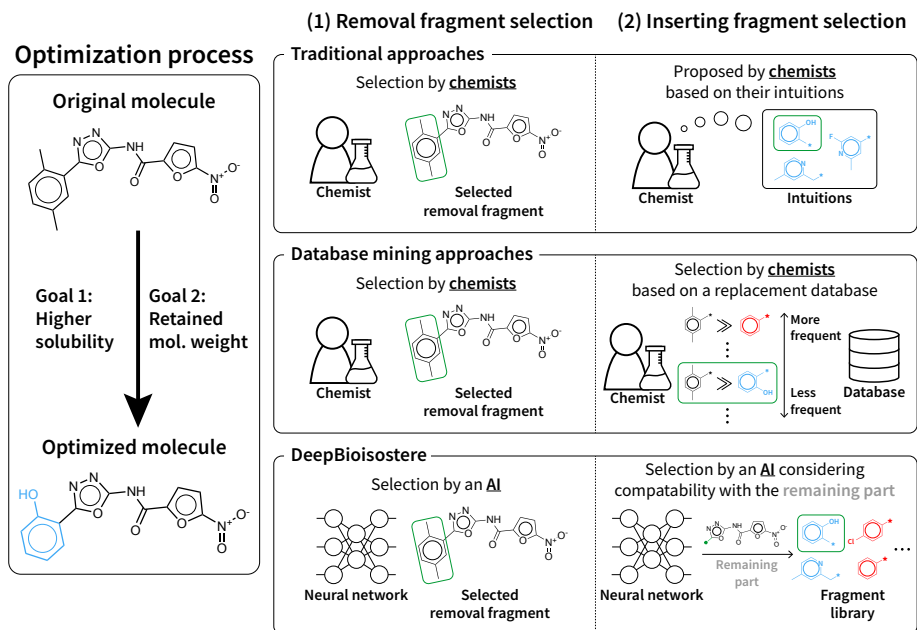


Fig. 1: An illustration of different approaches in bioisosteric replacement for given property optimization goals. Long-standing traditional approaches have relied on the knowledge of chemists for the entire optimization process. With an appropriate removal fragment selected by a chemist, one can employ traditional database-mining approaches to think of its various potential bioisosteres. Still, the intuition of experts is required to select the proper removal moiety for the property optimization goals. Unlike the previous approaches, which inevitably depend on the intuition of experts, DeepBioisostere utilizes a neural network to mimic the sequential decision-making process of the molecule optimization process based on bioisosterism. By taking into account the entire molecular structure, DeepBioisostere can flexibly suggest modified molecules that satisfy the delicate property control conditions.

fragment selection, and (3) attachment orientation prediction. These three steps are sequentially applied to complete molecular optimization. To achieve desirable structural modification, target biochemical properties dictated by the molecular structure should be considered during the three steps. For this purpose, we devised a deep generative model named DeepBioisostere to design a bioisosteric replacement for the multi-property control of a particular molecule.

The DeepBioisostere model is trained on an MMP dataset with structural analogs with minor differences, which we constructed from the ChEMBL database. Since we designed the model with three main modules corresponding to each step in the chemical modification process, it learns the proper ways to remove and then insert fragments

to meet the given conditions of multiple biochemical properties. This sequential modification facilitates the optimization of a molecule while retaining its overall properties, except for the target ones to be improved. Notably, the DeepBioisostere model comprises two embedding networks at different levels: atom and fragment. This unique feature, especially the latter network, enables the model to learn the compatibility between an insertion fragment and the remaining parts, allowing for fine control of complex properties that depend on the entire molecular structure. For synthetically accessible chemical modification, the DeepBioisostere model enumerates molecular fragments within a given molecule based on Breaking Retrosynthetically Interesting Chemical Substructures (BRICS)[42] rules, and selects one of them as a removal fragment. Then, the model selects an insertion fragment from a pre-defined fragment library by examining all of its items in terms of their compatibility with the remaining part of a given molecule and the target property control condition. More details about the training and generation processes of the DeepBioisostere model can be found in Section 4.

2.2 Multi-property Control with DeepBioisostere

We first apply our DeepBioisostere model to multi-property control tasks. During the optimization of a potent molecule in drug development, its structure is modified and elaborated to improve biochemical properties, such as lipophilicity, water solubility, synthetic accessibility, and drug-likeness. This so-called multi-property control is more challenging than controlling a single property since, for example, the lipophilicity can be increased simply by elongating a carbon chain, but the modified structure is often not drug-like.[43] Thus, a comprehensive consideration of the whole ligand structure and its properties is required to modulate multiple properties simultaneously.

Here, the goal is to provide modified molecular structures to meet a given multi-property condition. We tested our model for three scenarios that practitioners might encounter in a lead optimization process: (1) increasing or decreasing ligand lipophilicity while maintaining its molecular size, (2) increasing drug-likeness while maintaining its molecular weight, and (3) alleviating the synthetic complexity of a ligand with fair bioactivities. The second and third scenarios are more challenging than the first, which requires more comprehensive consideration of the relationship between the properties of interest. Throughout Section 2.2, the following criteria are commonly employed to select test molecules: (1) a single neutral molecule, (2) molecular weight that falls within the range of 100 to 500, and (3) inclusion of at least one BRICS bond. In addition, to examine our model’s capability to find novel bioisosterism, we only used fragments from the test dataset for insertion, which were never adopted either as ground truths or negative samples for the insertion step in the training process.

The overall property control results are exhibited in Table 1. For scenario 1, we selected 1,000 unique molecules whose $\log P$ values are within the range of 1 to 5, regarded as moderate lipophilicity. Whether one should increase a molecule’s $\log P$ or not depends on its specific application; for example, the biological target under consideration or the drug delivery plan are critical factors in making such a decision. Thus, we tested our model for both cases with two property control conditions: increasing $\log P$ by 1 and decreasing $\log P$ by 1 while maintaining overall molecule size in terms

Scenario	Requested Optimization		Property Change	
	Property	Δ Value	Average	Std. Dev.
Scenario 1	MW	0	+0.04	12.8
	$\log P$	+1	+0.83	0.38
	MW	0	-0.28	12.6
	$\log P$	-1	-0.84	0.43
Scenario 2	MW	0	-0.11	12.1
	QED	+0.1	+0.067	0.090
	MW	0	-0.57	12.0
	QED	+0.2	+0.100	0.099
Scenario 3	QED	0	-0.026	0.073
	SAscore	-0.5	-0.424	0.433
	QED	0	-0.028	0.074
	SAscore	-1.0	-0.719	0.524

Table 1: Results of three multi-property control scenarios. The requested optimization is the property control condition given to our model. For each scenario, we have two properties to control: Scenario 1 - modulating $\log P$ while maintaining MW. Scenario 2 - increasing QED while keeping the molecular weight. Scenario 3 - decreasing SAscore without losing QED. Δ Value is the requested property change in each property. Average and Std. Dev. designates the mean value of property change and its standard deviation, respectively.

of molecular weight (MW). We note that $\log P$ is a logarithm of the octanol-water partition coefficient, so the difference by 1 corresponds to a 10 times larger or smaller solubility ratio.[44] We generated ten unique molecular structures for each original molecule according to the two property control conditions. For a few test molecules, DeepBioisostere generated fewer than ten molecular structures for each one since the BRICS-allowed insertion fragments were fewer than ten. The results are summarized in the first row on Table 1. We observed that the mean values of the molecular weight differences between an original molecule and its modified ones were almost negligible: +0.04 and -0.28, respectively. These values suggest that the molecular weights of most modified structures are different from the original ones by less than one heavy atom. (See Supplementary Figure 4 for more details about property distributions) Meanwhile, $\log P$ was modulated with averaged changes of +0.83 and -0.84, falling slightly behind the requested property values. These statistics indicate that our model successfully adjusted the lipophilicity of the given molecular structures with barely changing their molecular weights, which requires careful selection of both removal and insertion fragments.

Second, we demonstrated an optimization process where a molecular structure is modified to improve its drug-likeness in terms of quantitative estimation of drug-likeness (QED).[45] (Scenario 2 in Table 1) In this scenario, only molecules whose QED values are less than 0.4 were used as test molecules. Property control conditions

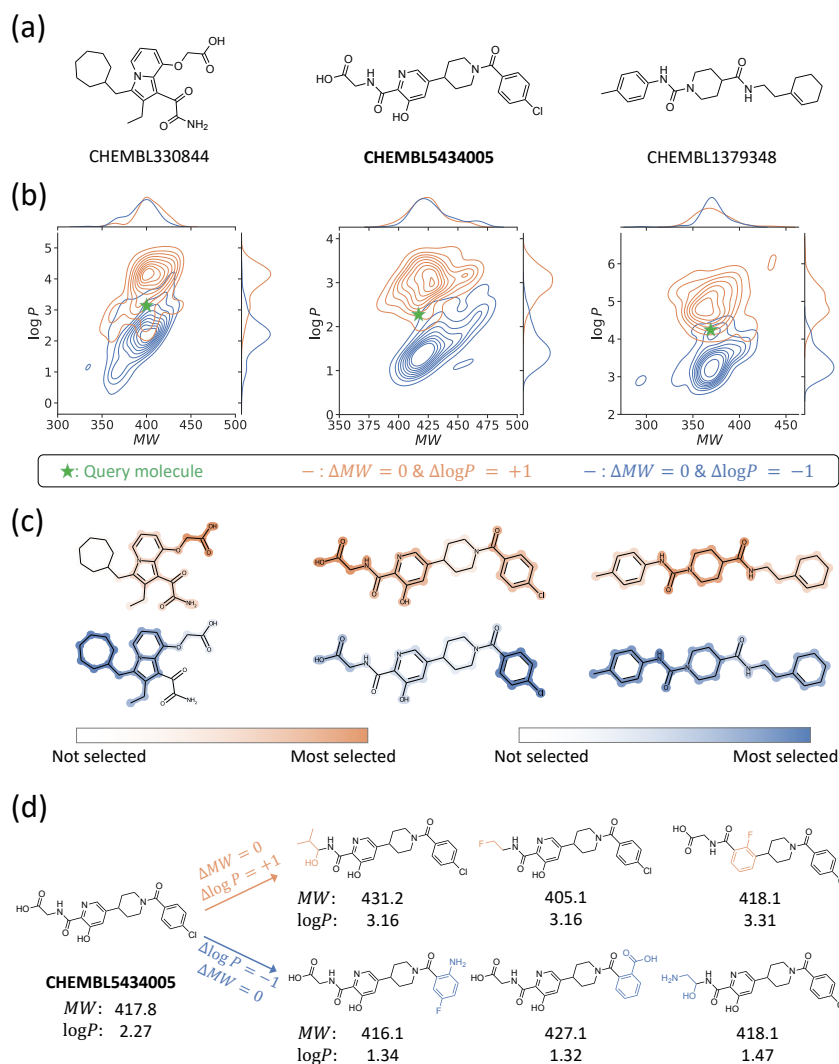


Fig. 2: Case studies on the multi-property control with DeepBioisostere for scenario 1, described in Table 1. In this figure, orange-colored ones are results for increasing $\log P$ by +1, and blue-colored ones are for decreasing $\log P$ by -1, both with maintaining molecular weights. (a) Three original molecules are to be modified. (b) Two-dimensional distribution plots of 100 unique modified molecules for each original molecule. (c) Removal fragment selection results. The thicker a fragment is shaded, the more it was chosen as a removal fragment for property control. The upper orange-colored ones visualize the results for increasing $\log P$, and the lower blue-colored ones visualize the results for decreasing $\log P$. (d) Two series of the top-ranked structures were derived from the second test molecule, CHEMBL5434005.

were set to increase the QED value by 0.1 or 0.2 while keeping the molecular weight constant. By employing the DeepBioisostere model, we were able to obtain novel molecules with enhanced drug-likeness; the mean values of QED changes were +0.067 and +0.100, respectively. This result indicates that our model can modulate drug-likeness without much change in the original molecular structure, which is critical in order not to lose pre-established crucial properties. Although the property control condition specifying a larger QED increase yielded molecules with higher QED values, the deviation from the given condition also became larger. It is not surprising that increasing QED by 0.2 is even more challenging, as the occurrence of such replacements within our training dataset is exceedingly rare. Refer to supplementary Section 4.1 for further discussion about the statistics.

Lastly, we tested our model to enhance the synthetic accessibility of a molecule with a high QED value but low synthetic accessibility. (scenario 3 in Table 1) Here, we adopted the SAScore introduced by Ertl and Schuffenhauer [46], a widely used estimator of synthetic accessibility. We collected test molecules for this scenario with the criteria that the QED value is greater than 0.7 and the SAScore is greater than 4. Note that the SAScore of a simple catalog molecule is about 2 or 3, whereas for a natural product, it is mostly greater than 5.[46] Property control conditions were set to decrease the SAScores of molecules by 0.5 or 1.0 while retaining their QED values. In this scenario, our model provided novel molecules with lower SAScores, although several of them exhibited somewhat decreased QED values. This result suggests that DeepBioisostere can be adopted to supplement many in silico methods for drug design, whose outcomes are often questioned regarding their synthetic accessibility.[47, 48]

2.3 Detailed Analysis on Modification with DeepBioisostere

In Section 2.2, we demonstrated that DeepBioisostere can control multiple molecular properties simultaneously while modifying molecular structures. Next, we analyze the modification process in detail in terms of two major steps: the removal fragment selection and the insertion fragment selection. Careful decisions in these steps are essential to control molecular properties, where the overall molecular structure is to be determined. Here, we carry out case studies for multi-property control and will discuss the removal fragment selection and the insertion fragment selection sequentially.

We randomly selected three molecules from the ChEMBL database with moderate molecular weight and lipophilicity, as visualized in Fig. 2(a). We suppose scenario 1 introduced in Section 2.2, where $\log P$ is to be modulated while a molecular weight is kept unchanged. We generated 100 unique modified molecular structures for each test molecule and property condition with the DeepBioisostere model. Again, only the fragments from the test dataset for insertion were adopted, the same as in the previous section. We exhibited their $\log P$ values and molecular weights in Fig. 2(b). For every test molecule, the generated structures under different property conditions showed distributions that were completely distinct in terms of $\log P$ values but very similar in molecular weights. $\log P$ was increased or decreased by about 1 while most changes in molecular weight were less than 20, corresponding to the weight of one or two heavy atoms.

2.3.1 Removal Fragment Selection

We looked into the generated molecules and analyzed the removal fragment selection step. We counted how many times each substructure was selected as a removal fragment and visualized them in Fig. 2(c). For the molecule in the middle column, ChEMBL5434005, the carboxylic acid group was most frequently selected as a removal fragment to increase $\log P$. In contrast, to decrease $\log P$, it was hardly substituted, but the chlorobenzene moiety was preferred as a removal fragment. These choices of removal fragments align well with the known chemical knowledge; introducing a carboxylic acid group enhances hydrophilicity, whereas incorporating an aryl halide moiety increases hydrophobicity. The other two test molecules also showed similar differences in the removal fragment selection under different property control conditions, as exhibited in the 1st and 3rd columns in Fig. 2.

We further visualized three analogs for ChEMBL5434005 generated by DeepBiosisostere with the highest likelihoods in Fig. 2(d). When conditioned to increase $\log P$ (orange arrow), the carboxylic acid group of the parent molecule was replaced with an isopropanol or fluoroethyl group, and the hydroxypyridine scaffold was substituted by a fluorobenzene ring, which are the cases where bioisosteric replacements that introduce more polarity were applied. As a result, the proposed molecular structures exhibited $\log P$ values higher than the original. Meanwhile, to reduce the $\log P$ value (blue arrow), our model selected the 4-chlorophenyl moiety on the terminal site of ChEMBL5434005 as a key site for modification. The chosen alternative fragments introduce more hydrophilic aryl groups, reducing the modified structures' $\log P$ values. In the last example, the DeepBiosisostere model selected a carboxylic acid group, despite its well-known hydrophilicity, as the removal fragment. We believe this is due to the fact that a carboxylic acid is one of the most frequently considered bioisosteres in the hit-to-lead process, which should be reflected in the training data we constructed.[49] Importantly, our model still succeeded in lowering the $\log P$ of the given molecule by introducing a more hydrophilic moiety as an alternative. These results suggest that our model's sequential-decision framework discussed in Section 2.1 effectively balances property-control objectives by choosing appropriate removal fragments and selecting insertion fragments conditioned on diverse combinations.

2.3.2 Insertion Fragment Selection - Effect of Chemical Environment on Property Control

Another essential factor that governs the selection of the insertion fragments is the chemical environment. Here, we refer to the chemical environment as the substituents surrounding the selected removal substructure to be replaced by a new insertion fragment. We demonstrate its importance in molecular optimization by two single-property control tasks: increasing $\log P$ by 1 and increasing QED by 0.1.

Fig. 3 illustrates the overall experimental procedure and its results. First, we selected two molecules that contain a pyrazole group, which is a frequently considered aromatic group in bioisosteric replacement.[7] Their molecular structures are shown in Fig. 3(a); we refer to them as molecules A and B (or M_A and M_B , respectively).

The two molecules exhibit great differences in $\log P$ (5.54 and -0.35) while showing moderate levels of QED values (0.42 and 0.41). Thus, the pyrazole moieties in the two molecules are situated in fundamentally different chemical environments, particularly in terms of the number of aromatic rings, hydrogen bond donors and acceptors, and rotatable bonds. Here, we forced our model to choose only the pyrazole groups as removal fragments to modulate a given target property, resulting in 100 unique modified structures. (M'_A and M'_B in Fig. 3(a)) For comparison, we retrieved the insertion fragments selected for molecule A and incorporated them into molecule B, resulting in another set of 100 unique molecules. (M''_B in Fig. 3(a)) In the first two cases, M'_A and M'_B , the individual chemical environments were directly engaged in the selection of insertion fragments. However, in the case of M''_B , the insertion fragments were selected based solely on the chemical environment of molecule A, without any involvement from molecule B. By comparing these cases, we can examine the significance of the chemical environment in molecular property control, especially during the selection of insertion fragments.

Fig. 3(b) and (c) show the property distributions of the modified molecules, where both M'_A and M'_B nearly achieve the objective values. However, in the case of M''_B , the observed property changes in $\log P$ and QED conditioning tasks were distinct. In the former task, insertion fragments selected to increase $\log P$ of molecule A also increased $\log P$ of molecule B, despite the differences in the chemical environments in which the pyrazole moieties were involved. Conversely, in the QED conditioning task, the case of M''_B resulted in molecular structures with decreased QED values, while those from M'_A and M'_B exhibited increased QED values compared to the original ones. This apparently shows that the bioisosteric replacements selected to improve the QED value of molecule A failed to improve that of molecule B. We attribute this distinction to the intrinsic difference between the two properties; $\log P$ can be readily approximated by summing over the estimated contributions of each chemical moiety in a molecule, while QED is a non-linear function of the molecule-level structural features, such as the numbers of hydrogen bond donors and acceptors. This example highlights the importance of considering the entire chemical environment, not just the removed fragment, when designing a suitable bioisosteric replacement for properties that depend on global molecular context. Such context-dependent property modulation cannot be handled by database-mining approaches, which rely solely on pre-defined fragment statistics. In contrast, DeepBioisostere explicitly learns to capture the non-linear relationships between fragments and their molecular environments, enabling context-aware bioisosteric replacements.

2.4 Exploring Bioisosteres for Uncommon Molecular Fragments

Next, we examine our model in identifying potential bioisosterism. Identification of novel bioisosteres becomes necessary when modification of an uncommon molecular fragment is required. In this case, a typical database-mining approach is likely to be insufficient since only a few bioisosteres from the database might be available for that fragment. Indeed, among 140,193 fragments in the fragment library we created, 98,459

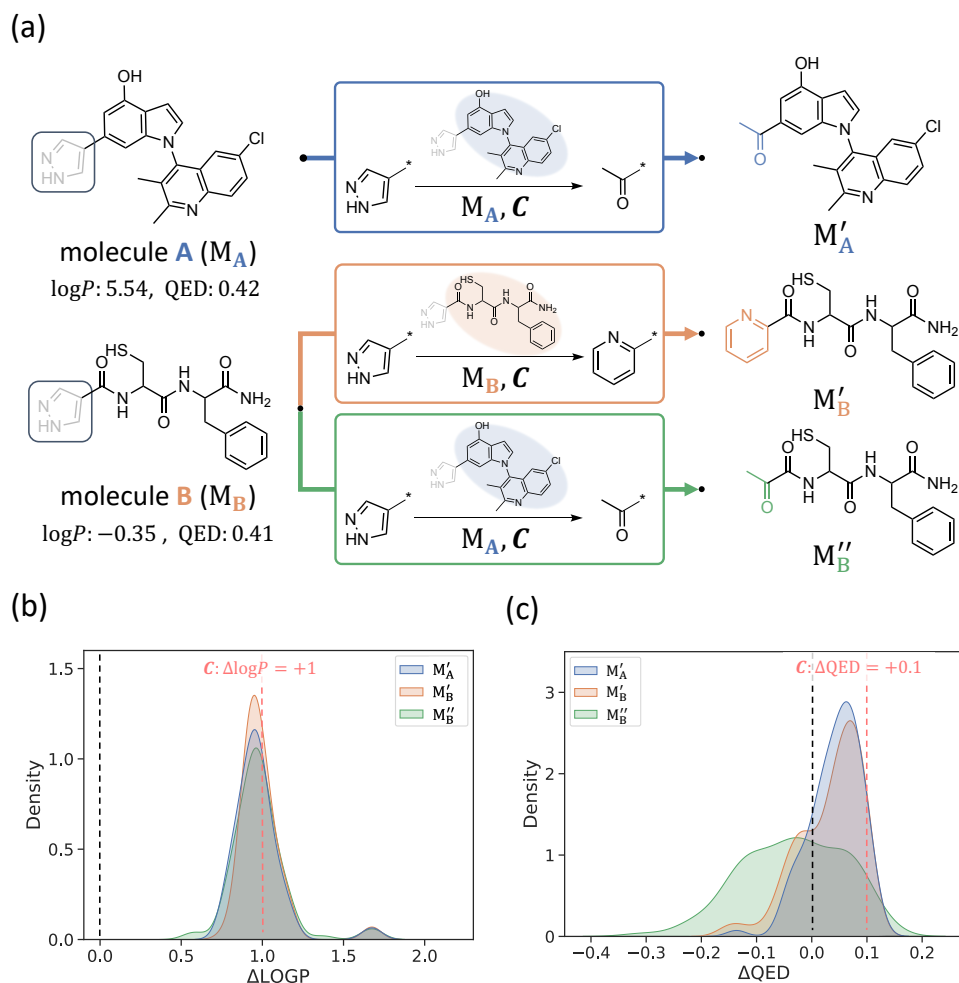


Fig. 3: An example showing the significance of chemical environment during insertion fragment selection. (a) Three replacement cases: within molecule A (M'_A), within molecule B (M'_B), and from molecule A to molecule B (M''_B). (b) $\Delta \log P$ distributions of modified molecules for each original molecule. (c) ΔQED distributions of modified molecules for each original molecule. In both (b) and (c), the black and red dashed lines denote the baseline implying original molecules' property values and property conditioning objectives, respectively.

fragments are found to have no more than ten bioisosteres, respectively. Fig. 4 illustrates such an example of modifying an uncommon fragment. The molecular fragment in Fig. 4(a), a 4-azaindole moiety, appears dozens of times in the ChEMBL database as a linker in the visualized fashion. Utilizing our MMP database, only four fragments were found as bioisosteres, and we visualized them in Fig. 4(b). All the found

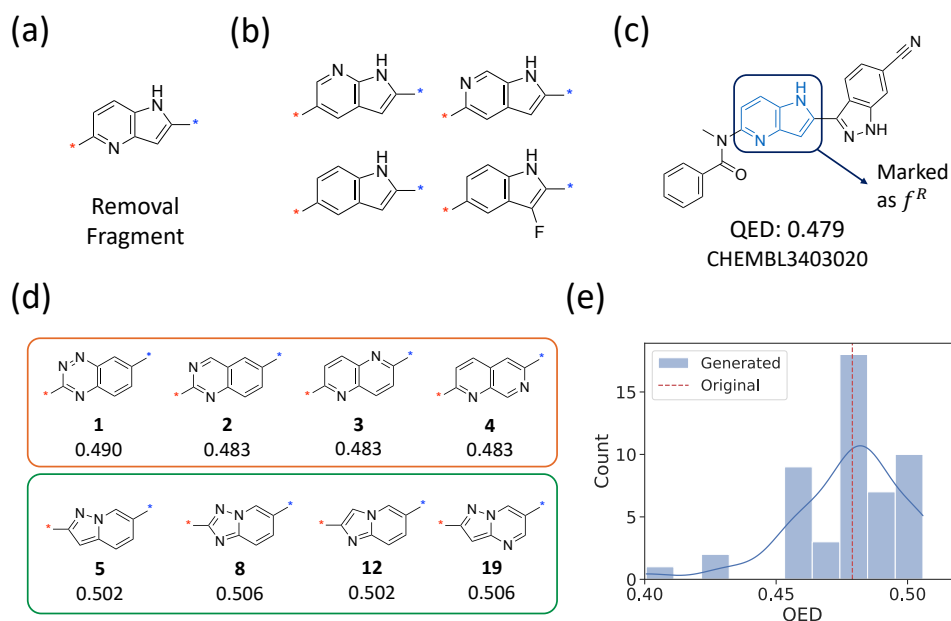


Fig. 4: An example to find bioisosteres of an uncommon molecular fragment. (a) A 4-azaindole moiety, an example of an uncommon moiety. (b) Bioisosteres of the 4-azaindole linker identified from our MMP database. (c) A test molecule from the ChEMBL database, which was modified by our model with its azaindole moiety marked as a removal fragment. (d) Eight top-ranked fragments proposed by our model as bioisosteres. The fragments fall into mainly two types, grouped by different colored boxes for each type. The integer placed below each fragment indicates the order ranked by the DeepBioisostere model, and the decimals are the QED values of the resultant molecules. In (a), (c), and (d), the red and blue stars (*) indicate the corresponding connection sites, respectively. (e) The QED distribution of the 50 generated molecules. The red dashed line denotes the QED value of the original molecule.

bioisosteres are fused aromatic heterocycles, the same as the original fragment except for one heavy atom, which can form similar non-covalent interactions with biological targets. However, by solely depending on these fragments identified from the MMPA, one cannot explore diverse structural analogues of an acclaimed molecule. More statistics about the number of bioisosteres for each fragment in the fragment library can be found in Supplementary Figure 3.

To find more bioisosteres beyond them, we employed our model on a molecule from the ChEMBL database by specifying the azaindole moiety as a removal fragment, as in Fig. 4(c). We allowed all the insertion fragments in our fragment library regardless of whether they were used in the training process. Here, to explore bioisosteres of the azaindole moiety that exhibit similar drug-likeness, we set the property control objective as $\Delta\text{QED}=0$. With this setting, we generated 50 unique molecular structures from the original molecule with DeepBioisostere.

Fig. 4(d) illustrates eight insertion fragments predicted by our model. Under the constraint of $\Delta\text{QED}=0$, several fused aromatic rings containing a few hetero-atoms were chosen as bioisosteres of the azaindole moiety. These fragments feature either a six-membered ring fused to a five-membered ring (the green box) or two six-membered rings, in contrast to the original azaindole moiety (the orange box). Despite this variation, all highly ranked fragments, when inserted into the test molecule, exhibit QED values comparable to the original. (see Fig. 4(d)) Each fragment retains a similar number of hydrogen bonding sites, two aromatic rings, and comparable lipophilicity, suggesting that they can engage in analogous non-covalent interactions. Fig. 4(e) illustrates the QED distribution of 50 unique modified structures. The peak near the original QED value implies that most insertions retain key biochemical features, including hydrogen-bond capacity, aromaticity, and polar surface area. This case study demonstrates that DeepBioisostere can be effectively applied to identify potential bioisosteres of uncommon chemical moieties that exhibit drug-likeness profiles comparable to those of the parent moiety.

2.5 In Silico Hit-to-lead Optimization of Structure-based Generative Model-derived Hit Candidates

We further extend the scope of our model to an in silico hit-to-lead workflow, where model-generated hit candidates are refined to improve drug-likeness and synthetic accessibility. Recent 3D molecular generative models for structure-based drug design have focused more on binding affinity to a given target protein, especially considering the structural context of the pocket environment in which the interaction between a protein and a generated molecule occurs.[50–53] Despite the target-specific design capacity of these approaches, generated molecules often fail to meet the criteria of experimental hits due to other molecular properties.

This gap between computational and actual hits highlights the need for a robust strategy to refine model-generated hit candidates, or in other words, to enhance molecular properties while preserving binding affinities. Hence, we demonstrate the synergy of using DeepBioisostere for multi-property optimization on top of target-specifically designed molecules from molecular generative models, revealing the applicability of our strategy. The goal here is to optimize synthesizability and drug-likeness of hit candidates, estimated as SAScore and QED, respectively, without losing their bioactivities towards respective targets.

We initially obtained computational hit candidates by four recent state-of-the-art structure-based 3D molecular generative models: Pocket2Mol[50], DeepICL[51], TargetDiff[52], and DecompDiff[53]. From the CrossDocked2020 test set, we selected three target proteins whose generated molecules exhibit both poor drug-likeness and synthetic accessibility, making them suitable targets that can take the most advantage from chemical modification. The details of the model used and the criteria for target selection, along with the statistics of the generated molecules, are provided in the Supplementary Information Section 7. Generated molecules for each target and model, termed computational hit candidates, underwent modifications through different replacement selection strategies, including DeepBioisostere. For comparison of our model with conventional database-mining methods, we adopted three baseline

replacement strategies, which are referred to as random, frequency-based, and MMPA-based, as shown in Table 2. The three strategies were set to utilize the bioisosteric pairs in the MMP database we constructed. In particular, the MMPA-based strategy first filters out replacements whose occurrence in our database is less than 10 times, and then selects replacements that exhibited the highest improvement in both QED and SAScore in the database. This process is based on statistical evidence in the MMP database, in the same way with the conventional database-mining strategies, such as SwissBioisostere. Here, we guide DeepBioisostere to increase QED by 0.1 and to decrease SAScore by 1.0, simultaneously. For each method, replacement was attempted 100 times for each input molecule.

Model	Strategy	Success Rate			
		QED	SAScore	Docking	Joint
DeepICL	Random	0.19	0.17	0.97	0.06
	Frequency-based	0.30	0.26	0.99	0.10
	MMPA-based	0.33	0.22	0.97	0.11
	DeepBioisostere	0.69	0.80	0.96	0.56
Pocket2Mol	Random	0.62	0.39	0.91	0.24
	Frequency-based	0.67	0.51	0.97	0.36
	MMPA-based	0.64	0.42	0.98	0.30
	DeepBioisostere	0.75	0.74	0.94	0.56
TargetDiff	Random	0.32	0.50	0.96	0.18
	Frequency-based	0.43	0.58	0.98	0.25
	MMPA-based	0.42	0.50	0.99	0.20
	DeepBioisostere	0.83	0.87	0.97	0.74
DecompDiff	Random	0.38	0.39	0.95	0.19
	Frequency-based	0.49	0.45	0.98	0.24
	MMPA-based	0.43	0.29	0.99	0.13
	DeepBioisostere	0.79	0.87	0.96	0.68

Table 2: Success rate of in silico hit-to-lead workflow. Starting from the model-derived hit candidates, four different replacement strategies are applied to achieve the goal of multi-property control—enhancing QED and SAScore while maintaining the docking score. The best success rate among strategies is highlighted in bold.

For evaluation, we compared the success rates of QED and SAScore optimization, as well as the retention of docking scores to a protein target. The success criteria for QED and SAScore are based on whether the generated molecule exhibits better properties than the original. We consider a generated docking score as a success when it is retained during replacement within 1.36 kcal/mol, corresponding to a 10-fold change in IC₅₀. The most integral metric, which is termed ‘Joint’, means the ratio of generated molecules jointly meets all the aforementioned criteria—improved QED, SAScore, and

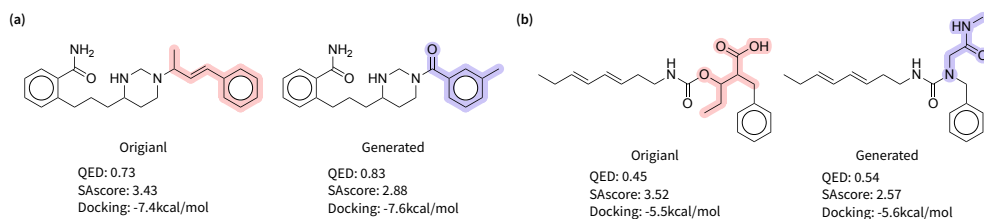


Fig. 5: Examples of generated molecules by DeepBioisostere for Table 2. The original molecules are selected from the generation results of DeepICL[51] on target 4RV4.

preserved docking score—thereby indicating the success in the computational hit-to-lead scenario for increasing synthesizability and drug-likeness.

Table 2 shows the result of a target protein with PDB ID 4RV4, whereas the other results are shown in the Supplementary Table 4. Although frequency- and MMPA-based strategies performed well at docking score retention—possibly as a result of the use of our bioisosteric replacement library curated from bio-assays—DeepBioisostere mostly achieved superior performance in optimizing the properties such as QED and SAScore. We attribute the improved controllability of QED and SAScore to the consideration of the entire molecular graph, along with the removal and insertion fragments, rather than focusing solely on a single fragment as in the baselines. The true power of DeepBioisostere is demonstrated in its ability to satisfy all criteria simultaneously, as evidenced by its superior performance in the ‘Joint’ metric, for which baseline approaches exhibited less than 10 % success.

Figure 5 shows two example molecules generated based on bioisosteric replacements identified by DeepBioisostere, both of which achieve improved QED and SAScore while preserving the binding affinity of the original molecule. Notably, these improvements arise from the substitution of the fragments resulting in amide-containing molecule, which is expected to enhance the synthetic accessibility. Together, this robust ability to find replacements that fulfill multiple objectives is notably agnostic to underlying generative models, establishing it as a broadly applicable and powerful strategy for in silico drug design.

3 Discussion

In this work, we propose a deep generative model named DeepBioisostere for autonomous bioisosteric replacement with fine control over multiple molecular properties. Our model conducts chemical modification in an end-to-end manner, from selecting fragments to remove and insert, along with their attachment orientation. We demonstrate various scenarios of dual property control, where one property is altered while the other remains unchanged. DeepBioisostere successfully modulated the properties of the given molecules in all scenarios by replacing the fragments in the desired manner. We further demonstrate the adjustability of DeepBioisostere, which dynamically selects the fragment to remove based on the given property control condition. This is practically advantageous, where previous database-mining approaches heavily

rely on the help of experts for choosing a substructure to be modified. Moreover, we justify the significance of substituents near the replacement site in controlling comprehensive molecular properties, especially for the selection of insertion fragments, which could not be addressed by conventional in silico approaches. Our model enables more diverse replacements appropriate for the given property condition, extending from the existing moiety pairs within the database. We emphasize that this is particularly important when the removal fragment is uncommon, as it provides a wide variety of potential chemical modifications. Finally, we applied DeepBioisostere to a practical scenario that mimics the hit-to-lead process, which involves optimizing the drug-likeness and synthetic accessibility of computationally generated hit compounds while retaining their binding affinities. These results demonstrated that DeepBioisostere successfully tuned multiple properties without disrupting binding affinity for all 3D molecular generative models used, showcasing the promising role of our approach in autonomous drug design.

While DeepBioisostere already demonstrates the ability to control multiple molecular properties through a deep generative framework, its design also opens promising directions for further enhancement. In particular, extending the model with multi-task and transfer learning could enable it to handle conditions with limited or noisy labels more effectively. Pretraining on widely available or easy-to-label molecular properties, such as QED, logP, and SA score, and transferring the learned representations to tasks involving complex endpoints, like ADMET properties, would enable the framework to generalize across a broader chemical and biological space. Such advancements could further strengthen the model’s applicability to diverse drug discovery pipelines, facilitating more accurate and data-efficient molecular design in increasingly realistic and challenging scenarios.

4 Methods

4.1 Finding Molecular Pairs with Bioisosterism: Dataset construction

In this section, we present our scheme for constructing a training dataset. It is a pivotal step in our work, where the dataset should be precisely tailored to align with the objective of DeepBioisostere. To obtain a dataset with potential bioisosteric replacements, we begin from the ChEMBL database[26] and go through two steps of training dataset construction: pre-filtration and MMP identification.

4.1.1 Pre-filtration

We adopted a permissive pre-filtration strategy to maximally retain the data. Simply, we excluded heavy molecules with molecular weights exceeding 800 Da and molecules consisting of salts. Additionally, molecules with an inhibitory concentration greater than 10 μM are also excluded so that the remaining molecules can be regarded as possessing sufficient bioactivities. This pre-filtration process provides a refined dataset appropriate to the next stage of MMP identification. From the total of 4,182,178 ChEMBL molecules, we were able to obtain 1,054,335 molecules by pre-filtration.

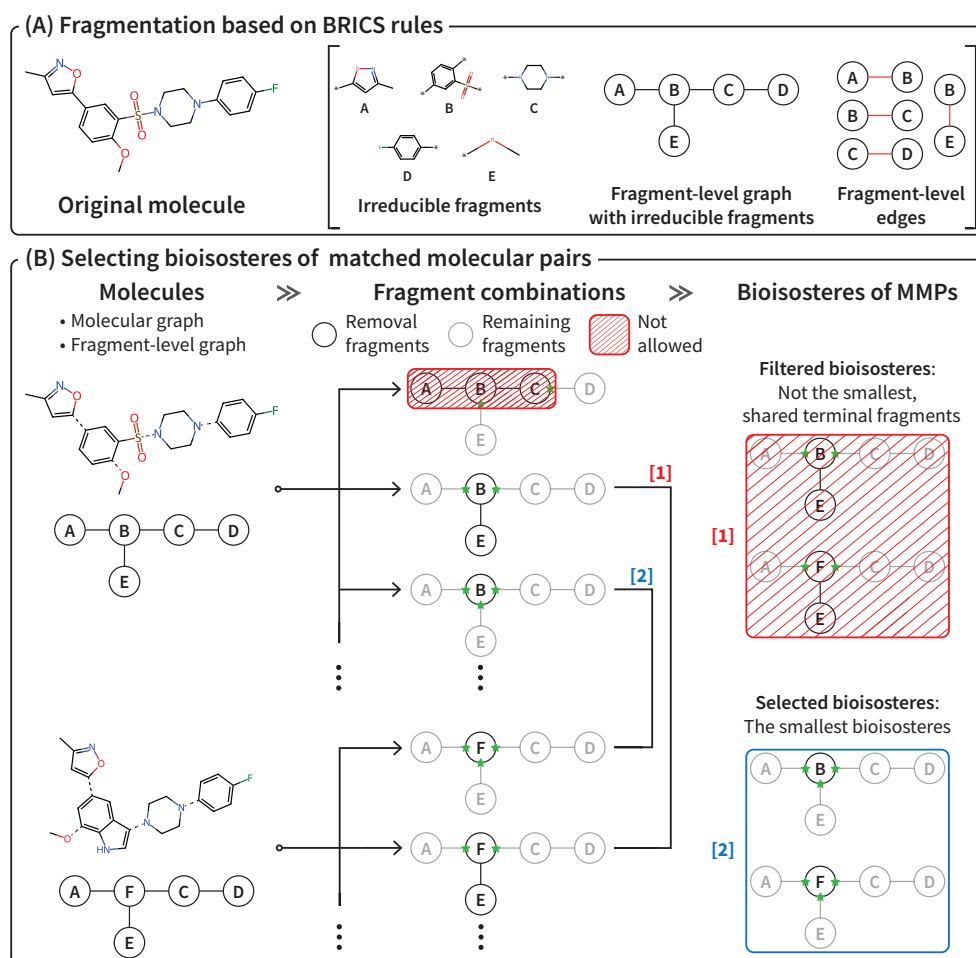


Fig. 6: The overall dataset generation scheme. (a) The original molecule is fragmented according to the BRICS rules to derive irreducible fragments, resulting in a fragment-level graph with the corresponding edges, where each edge corresponds to a single BRICS bond. (b) The dataset is constructed by identifying bioisosteres. First, allowed fragment combinations are extracted for each molecule. Then, the smallest bioisosteres are selected for each matched pair of molecules that share the remaining fragments. The dataset incorporates all selected bioisosteres, along with the original molecule, the modified molecule, and the bioisostere pair representing the removal and insertion fragments.

4.1.2 Identifying Bioisosteric Replacements based on the BRICS MMPs

MMP is a pair of molecules in which all parts are identical except for a small fragment in each molecule. From the pre-filtered ChEMBL database, we identified MMPs

by fragmenting each molecule and then selecting molecule pairs that share common fragments. It is crucial to adopt a proper fragmentation rule in this process since it determines the fragments corresponding to the *difference* between each MMP, which are to be considered potential bioisosteres. To consider more synthetically accessible modifications than the conventional strategy of simply cleaving rotatable bonds in the fragmentation process, we employed BRICS[42] rules for molecular fragmentation, implemented in the RDKit[54] package.

Using the BRICS rules, the ChEMBL molecules are represented as fragment-level graphs (see Fig. 6(a)). Each node is *irreducible fragment*, a subgraph of a molecule that cannot be further divided via fragmentation, where edges between nodes correspond to the BRICS bonds. In this regard, a *removal fragment* is defined as a single subgraph of a fragment-level molecular graph. With these definitions, we enumerate multiple fragment combinations that involve a single removal fragment and remaining fragments for each BRICS-fragmented molecule. The fragment combinations are further filtered with two criteria about their removal fragments: (1) a maximum of 12 heavy atoms in a removal fragment, and (2) the removal fragment should have fewer heavy atoms than the remaining fragments.

The aforementioned process results in an enormous number of fragment combinations derived from diverse molecules. Then, the obtained fragment combinations are subsequently compared, where any molecular pairs with the same residual fragments are classified as MMPs along with their removal fragments. We note that the majority of the resultant MMPs contain more than two matched fragment combinations. For these cases, we exclusively selected the smallest removal fragments as bioisosteres (see Fig. 6(b)) This selection of the smallest removal fragment distinguishes our training dataset from previous database-mining approaches that enumerate every bioisosteric pair, preventing the accumulation of redundant data in the training data. To ensure that only MMPs preserving bioactivity were considered, pairs with $|\Delta_{\text{pChEMBL}}| > 1$ were filtered out. The final training dataset consists of a total of 2,874,580 MMPs specified about their corresponding bioisosteres.

Based on the final dataset, we collect the insertion fragments to build a *fragment library*. The fragment library is necessary for both the training and inference phases of DeepBioisostere as a source of insertion fragment candidates, which our model can utilize to optimize a given molecule. For more details on the use of the fragment library of DeepBioisostere, refer to the Sections 4.3 and 4.4. Note that gathering all removal fragments will result in the same fragment library since each identified MMP results in two training data entries with reverse relationships in their removal and insertion fragments. The resulting fragment library is composed of 140,096 diverse fragments. Furthermore, we randomly split the fragment library at a ratio of 8:1:1, leading to 112,076, 14,013, and 14,007 fragments for training, validation, and test datasets, respectively.

4.2 DeepBioisostere: Deep Generative Modeling of Bioisosterism

We designed DeepBioisostere to optimize a molecule through three essential steps involving the selection of (1) the removal fragment, (2) the insertion fragment, and (3)

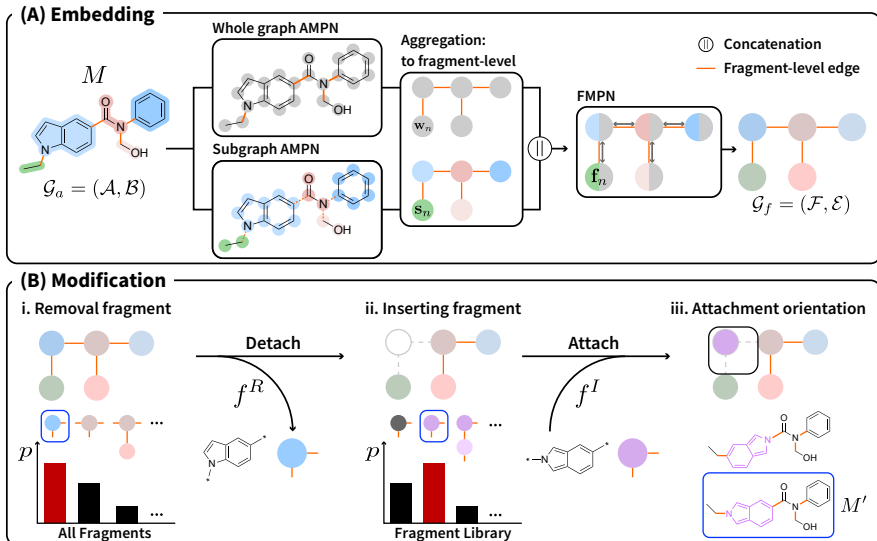


Fig. 7: Operation scheme of DeepBioisostere. (a) Fragment-level feature embedding process. The original molecule, M , initially propagates through the whole graph and subgraph AMPN (atom message passing network). Subsequently, the atom-level embedding vectors are aggregated into a single fragment-level embedding vector, followed by an FMPN (fragment message passing network). (b) Based on the fragment-level vectors, DeepBioisostere sequentially selects the removal fragment, the insertion fragment, and the attachment orientation of the insertion fragment. The removal fragment is selected from all possible fragments of M , and the insertion fragment is chosen from our fragment library.

the attachment orientation. This sequential modeling was inspired by the traditional chemical modification process based on bioisosterism. With this perspective, we define a chemical modification task as learning the joint distribution, $p(M, M', \mathbf{C})$, of an original molecule, M , a modified molecular structure, M' , and a property control condition, \mathbf{C} . We factorize the joint probability with $p(M, M', \mathbf{C}) = p(M, \mathbf{C}) \cdot (M'|M, \mathbf{C})$. The joint probability $p(M, \mathbf{C})$ is the likelihood of the combination of an original molecule to be modified and a property control objective for that molecule, arising from former experimental observations. Therefore, we devise a generative model for the conditional probability, $p(M'|M, \mathbf{C})$, implying the likelihood of a modified structure to achieve the given property control condition starting from an original structure.

Depending on the fragmentation rule, \mathbf{R} , which defines what bond can be cleaved, the probability distribution must be different since achievable molecular structures from a single molecule would be different. For example, if we do not allow the cleavage of the single bond connecting aromatic rings, we cannot obtain phenyl aniline by modifying a biphenyl compound. Thus, we denote the objective conditional probability of our model as $p_{\mathbf{R}}(M'|M, \mathbf{C})$, reflecting the dependence of the chemical modification task on the bond cleavage rule, \mathbf{R} . For an MMP according to \mathbf{R} , (M, M') ,

their conditional probability can be reformulated by factorization with the conditional probabilities of corresponding three modification components as follows:

$$\begin{aligned}
 p_{\mathbf{R}}(M'|M, \mathbf{C}) &= p_{\mathbf{R}}(f^R, f^I, A|M, \mathbf{C}) \\
 &= \underbrace{p_{\mathbf{R}}(f^R|M, \mathbf{C})}_{(1)} \cdot \underbrace{p_{\mathbf{R}}(f^I|M, f^R, \mathbf{C})}_{(2)} \cdot \underbrace{p_{\mathbf{R}}(A|M, f^R, f^I, \mathbf{C})}_{(3)}, \quad (1)
 \end{aligned}$$

where f^R is a removal fragment, f^I is an insertion fragment, and A is an attachment orientation. Note that for a modification of M to M' , there might be more than one set of the three modification components, but we uniquely defined f^R and f^I to be only the smallest removal and insertion fragments in the training data construction procedure, respectively. In this way, the ground truth for $p_{\mathbf{R}}(f^R, f^I, A|M, \mathbf{C})$ is defined to be zero if f^R and f^I are not the smallest ones to modify M to another molecular structure, M' . Since the smallest structural change can always be identified from any MMP, this choice does not impose any restriction on the probability distribution of $p_{\mathbf{R}}(M'|M, \mathbf{C})$. The details about how we model each conditional probability of the Eq. (1) are discussed in Section 4.2.2.

4.2.1 Fragment-level Molecular Encoding

The overall framework of DeepBioisostere is depicted in Fig. 7. First, we encode an original molecule to be modified into fragment-level embedding vectors. We adopt a hierarchical architecture to facilitate probability modeling at the fragment level. An original molecule is represented in two ways: an atom-level graph G_a and a fragment-level graph G_f .

We adopted the core architectural design of Modof proposed by Chen et al. [38], which demonstrates strong molecular property conditioning performance through a hierarchical framework. In its design, as illustrated in Fig. 7, atom-wise embeddings are first generated using an atom-level graph message passing network, then aggregated into fragment-level hidden vectors, which are subsequently processed by a fragment-level graph message passing network. In DeepBioisostere, these two message passing networks are adapted for bioisosteric replacement and are referred to as the atom message passing network (AMPN) and fragment message passing network (FMPN), respectively.

To tailor the model for bioisosteric replacement, we design the AMPN with two submodules having distinct parameters: a whole-graph AMPN operating on all molecular nodes and a subgraph AMPN operating only within individual fragments. The subgraph AMPN is employed as a shared fragment embedder for both the original molecule and the fragment library, providing a consistent and comparable representation of molecular fragments. This weight-sharing strategy ensures a comprehensive understanding of fragments and, in turn, allows the overall generative model to be formulated as a product of fragment-level conditional probabilities (Eq. (1)). In contrast to Modof, which decodes new fragments independently from separate latent vectors, DeepBioisostere evaluates candidate replacements by directly comparing the

joint embedding of the removal fragment and each candidate insertion fragment from its library in this shared space. Furthermore, when combined with our same-bioassay molecular pair dataset, this molecular encoding strategy enables the model to capture similarity in bioactivity as well as differences in other molecular properties. We quantitatively analyze the contribution of this architectural design to multi-property optimization in Supplementary Information Section 5.1.

An initial atom feature vector, $\hat{\mathbf{a}}$, is concatenated with the condition vector, \mathbf{C} , to yield an input atomic embedding vector by $\mathbf{a}_i^0 = [\hat{\mathbf{a}}_i \| \mathbf{C}_i]$. Details about constructing the initial atom feature vectors are summarized in the Supplementary Information. We summarized key notations for model architecture in Table 3. Embedding vectors for both atoms and bonds are propagated through the AMPN layer as follows:

$$\mathbf{m}_i^t = \sum_{a_j \in \mathcal{N}(a_i)} W_1^a \mathbf{a}_j^t + W_2^a \mathbf{b}_{ij}, \quad (2)$$

$$\mathbf{a}_i^{t+1} = \text{GRU}(\mathbf{a}_i^t, \mathbf{m}_i^t), \quad (3)$$

where $\mathcal{N}(a_i)$ is neighboring atoms of a_i , GRU is the gated recurrent unit introduced in Chung et al. [55] The whole graph AMPN operates on the entire molecular graph \mathcal{G}_a , updating atom-level embeddings based on the collective information of all atoms and bonds in the molecule. In contrast, the subgraph AMPN works locally within each irreducible fragment, focusing its update on atoms only within the specific fragment, denoted as $\mathcal{A}(\hat{f})$. This subgraph-based update strategy allows the model to learn the comprehensive features of each irreducible fragment for further hierarchical message passing.

The updated atomic embedding vectors are aggregated into fragment-level embedding vectors for each irreducible fragment as follows:

$$\mathbf{w}_n = \sum_{a_i \in \mathcal{A}(\hat{f}_n)} \mathbf{a}_i, \quad (4)$$

$$\mathbf{e}_{nm} = \sum_{a_i \in \mathcal{A}(e_{nm})} \mathbf{a}_i, \quad (5)$$

where \mathbf{w}_n denotes a fragment-level embedding vector aggregated from the whole graph AMPN embeddings. Atom-level embeddings from the subgraph AMPN are aggregated in the same way, which is denoted as \mathbf{s}_n . Given that the subgraph AMPN updates the vectors without considering the information of adjacent atoms connected by the BRICS bonds, we exclusively employ the whole graph AMPN to aggregate the edge vectors of fragment-level graphs. We concatenate the two aggregated fragment-level embedding vectors for further propagation in FMPN, which incorporates the feature vector of each fragment and intrinsically works like AMPN:

$$\mathbf{m}_n^t = \sum_{\hat{f}_m \in \mathcal{N}(\hat{f}_n)} W_1^f \mathbf{f}_m^t + W_2^f \mathbf{e}_{nm}, \quad (6)$$

$$\mathbf{f}_n^{t+1} = \text{GRU}(\mathbf{f}_n^t, \mathbf{m}_n^t). \quad (7)$$

Notation	Description
$\mathcal{G}_a = (\mathcal{A}, \mathcal{B})$	Atom-level molecular graph
\mathcal{A}, \mathcal{B}	Set of atoms and bonds in \mathcal{G}_a , respectively
$a \in \mathcal{A}$	An atom in \mathcal{G}_a
$b_{ij} = \{a_i, a_j\} \in \mathcal{B}$	A bond connecting atoms a_i and a_j in \mathcal{G}_a
\mathbf{a}_i^t	An embedding vector of a_i in t^{th} layer
\mathbf{b}_{ij}	An embedding vector of b_{ij}
$\mathcal{G}_f = (\mathcal{F}, \mathcal{E})$	Fragment-level molecular graph
\mathcal{F}, \mathcal{E}	Set of irreducible fragments and edges in \mathcal{G}_f , respectively
f	A subgraph, fragmented by the BRICS rules
\hat{f}	An irreducible fragment
f^R	A <i>removal</i> fragment
f^I	An <i>insertion</i> fragment
$e_{nm} \in \mathcal{E}$	An edge between irreducible fragments \hat{f}_n and \hat{f}_m in \mathcal{G}_f , corresponding to a BRICS bond in \mathcal{G}_a
$\mathcal{A}(f)$	A set of atoms included in a subgraph f
$\mathcal{A}(e_{nm})$	A set of atoms composing e_{nm}
$\mathcal{F}(f)$	A set of irreducible fragments included in a subgraph f
\mathbf{f}_n^t	An embedding vector of \hat{f}_n in t^{th} layer
\mathbf{e}_{nm}	An embedding vector of e_{nm}
\mathbf{h}_f	An aggregated vector for f
A	An attachment orientation, a set of edges enumerated based on the BRICS rules
$[\cdot \parallel \cdot]$	Element-wise concatenation
σ	Sigmoid activation function
W	Learnable weights

Table 3: Notations and the corresponding descriptions in this work

Here, $\mathbf{f}_n^0 = [\mathbf{w}_n \parallel \mathbf{s}_n]$, is an initial feature vector of an irreducible fragment. The resulting fragment-level embedding vectors, $\{\mathbf{f}_n\}$, are utilized for the modification of M . Among the overall embedding process, the subgraph AMPN is significant since it allows DeepBioisostere to generate embedding vectors for previously unseen fragments.

With the fragment-level embedding vectors obtained by AMPN and FMPN, we model each conditional probability of Eq. (1). During the substitution, both f^R and f^I can be a combination of multiple irreducible fragments. Thus, we obtain the final embedding vector for each individual fragment through the aggregation of the involved irreducible fragments as follows:

$$\mathbf{h}_f = \sum_{\hat{f}_n \in \mathcal{F}(f)} \mathbf{f}_n. \quad (8)$$

We note that \mathbf{h}_f contains comprehensive information about the chemical structure of f , its relationships with surrounding fragments, and the given property control condition.

4.2.2 Modeling Sequential Modification Steps

With the aggregated embedding vectors, the DeepBioisotere model sequentially modifies the original molecule, M (see Fig. 7(B)). First, the removal fragment selection module estimates the probability of removing each fragment. This exclusively considers the allowed removal fragments, satisfying the criteria used during dataset construction, as detailed in Section 4.1. For a potential removal fragment f , the likelihood is formulated as follows:

$$p(f|M, \mathbf{C}) \propto \sigma(\phi(\mathbf{h}_f; \theta_R)), \quad (9)$$

where $\phi(\cdot; \theta_R)$ is a removal fragment selection module parameterized with θ_R . After the removal fragment is determined, our insertion fragment selection module chooses an appropriate fragment from the predefined library established during dataset generation. The following likelihood guides this selection:

$$p(f|M, f^R, \mathbf{C}) \propto \sigma(\phi([\mathbf{h}_{f^R} \parallel \mathbf{h}_f]; \theta_I)). \quad (10)$$

Similarly, $\phi(\cdot; \theta_I)$ is an insertion fragment selection module parameterized with θ_I . Thus, the insertion fragment depends on the pre-selected removal fragment, its surroundings, and the given property control condition, which are comprehensively included in \mathbf{h}_{f^R} . This contrastive formulation enables the model to explicitly learn bioisosteric relationships between fragments.

For an insertion fragment with two or more attachment sites, more than one *attachment orientations* might be allowed. For example, isoindole in the left side of Fig. 7(B) can be attached to the remaining substructure in two different orientations. In these cases, a proper attachment orientation should be determined to insert the selected fragment for desired property control. We enumerate all attachment orientations that are allowed by the BRICS rules, and then the last module estimates their likelihood:

$$p(A|M, f^R, f^I, \mathbf{C}) \propto \prod_{e_{nm} \in A} \sigma(\phi(\mathbf{e}_{nm}; \theta_A)), \quad (11)$$

where A is an attachment orientation, and $\phi(\cdot; \theta_A)$ is an attachment orientation selection module parameterized with θ_A . Eq. (11) indicates that each attachment orientation is evaluated based on the respective attaching sites (or edges) under the assumption that the compatibility of joining two fragments mainly depends on the local relationship.

4.3 Training DeepBioisostere

As explained in section 4.2.2, DeepBioisostere modifies a given molecule with three main modules. To learn the conditional distribution $p(M'|M, \mathbf{C})$ with them, we devised three loss functions for each module, $\mathcal{L}_{\text{remove}}$, $\mathcal{L}_{\text{insert}}$, and $\mathcal{L}_{\text{attach}}$, respectively. Then, we trained our model with their summation as the final training loss function.

The dataset constructed in Section 4.1 includes only positive data of the ground-truth removal fragment, insertion fragment, and attachment orientation. To make the

removal fragment selection module likely select the positive removal fragment over others, we regard other allowed fragments of the original molecule as negative samples for each pair of bioisosteres in the dataset. We employed the binary cross-entropy loss to formulate $\mathcal{L}_{\text{remove}}$ as follows:

$$\mathcal{L}_{\text{remove}} = -\log p_{\text{pos}}^R - \frac{1}{N_R} \sum_{f_{\text{neg}}^R} \log(1 - p_{\text{neg}}^R), \quad (12)$$

where $p_{\text{pos}}^R = \sigma(\phi(\mathbf{h}_{f_{\text{pos}}^R}; \theta_R))$, $p_{\text{neg}}^R = \sigma(\phi(\mathbf{h}_{f_{\text{neg}}^R}; \theta_R))$, f_{neg}^R is an allowed but negative fragment from the original molecule, and N_R is the total number of allowed but negative fragments from the original molecule.

The selection of insertion fragments is more complicated since our model should be able to retrieve the ground truth one among a vast number of potential ones from the fragment library. To avoid the inefficiency in evaluating tens of thousands of fragments for every data point, we employed the *negative sampling* strategy inspired by Seo et al. [56] This strategy samples only a few fragments (20 fragments in this work) with the probability weakly proportional to their occurrence as negative samples. With this negative sampling strategy, we formulated $\mathcal{L}_{\text{insert}}$ as follows:

$$\mathcal{L}_{\text{insert}} = -\log p_{\text{pos}}^I - \frac{1}{N_I} \sum_{f_{\text{neg}}^I} \log(1 - p_{\text{neg}}^I), \quad (13)$$

where $p_{\text{pos}}^I = \sigma(\phi([\mathbf{h}_R \parallel \mathbf{h}_{f_{\text{pos}}^I}]; \theta_I))$, $p_{\text{neg}}^I = \sigma(\phi([\mathbf{h}_R \parallel \mathbf{h}_{f_{\text{neg}}^I}]; \theta_I))$, N_I is the number of negative samples for each positive data. By including negative samples in Eq. (13), we counteracted the bias towards always preferring more frequently occurring fragments over less frequent ones. One potential concern is that, for a given molecular structure and its removal fragment pair, if there are two distinct ground-truth insertion fragments, one could mistakenly be sampled as a negative fragment during training. However, since the final training objective is defined as the expectation over the entire dataset, the model will ultimately assign equal probabilities to both fragments.

According to Eq. (11), we estimate the probability of each attachment orientation as the product of the likelihood of the potential edges to be formed from the attachment. Hence, we devised an edge-based objective function to train the attachment orientation selection module. For each positive data, we enumerate all the potential edges allowed by the BRICS rules and classify them into positive and negative ones according to whether they are included in the ground-truth attachment orientation. Then, we again set the binary cross-entropy loss in this task:

$$\begin{aligned} \mathcal{L}_{\text{attach}} = & -\frac{1}{N_{\text{pos}}} \sum_{e_{nm}^{\text{pos}}} \log p_{\text{pos}}^A \\ & - \frac{1}{N_{\text{neg}}} \sum_{e_{nm}^{\text{neg}}} \log(1 - p_{\text{neg}}^A), \end{aligned} \quad (14)$$

where $p_{pos}^A = \sigma(\phi(\mathbf{e}_{nm}^{pos}; \theta_A))$ and $p_{neg}^A = \sigma(\phi(\mathbf{e}_{nm}^{neg}; \theta_A))$. N_{pos} and N_{neg} are the numbers of potential edges within the positive and negative orientations, respectively.

For training and validation, we split the whole dataset constructed in Section 4.1 into training, validation, and test sets with a ratio of 8:1:1. The dataset was split according to their insertion fragments so that the three sub-sets share no insertion fragment. Thus, each dataset contains distinct bioisosteric replacements. For the multi-property control, we used a total of four properties that can be readily computed based on the structure of a molecule: molecular weight, $\log P$, QED,^[45] and SAScore.^[46] The training was finished in no more than 17 hours with a single NVIDIA RTX A4000 GPU for each property control condition. Details about the training process can be found in the Supplementary Information.

4.4 Molecular Optimization Process with DeepBioisostere

DeepBioisostere performs optimization with two inputs: a molecule to be improved and a property control condition. The molecule is first analyzed with the BRICS rules to obtain its fragment-level graph, and all its substructures are enumerated. Then, we filter the substructures based on the criteria used to identify MMPs in Section 4.1.2, allowing the modification to occur in a small part of the molecule. Thus, a substructure that contains more than 12 heavy atoms or more heavy atoms than the other parts of the molecule is not considered in the removal fragment selection. All the allowed fragments are examined by the removal fragment selection module, yielding likelihoods for each fragment. Based on the multinomial distribution, removal fragments are sampled according to the desired number of modified structures.

For each selected removal fragment, DeepBioisostere explores the fragment library to find suitable insertion fragments for property control. Since the chemical modification of a certain part should retain its surroundings, molecular fragments with different numbers of fragmented sites are not considered. In addition, among the corresponding fragments, only those that satisfy the BRICS rules at the respective removal site of the original molecule are considered. All the passed insertion fragments are then evaluated by the DeepBioisostere model, and the top insertion fragments are greedily selected. We note that, during the insertion fragment selection, either the occurrence data from the MMP database we created or from public chemical libraries, such as ChEMBL, is not utilized because the differences in occurrence are implicitly captured during the training process.

Lastly, the selected insertion fragments are examined in their attachment orientation. The combinations between the fragmented sites of the insertion fragment and its surroundings are enumerated and then filtered using the BRICS rules. The passed combinations are then prioritized by the DeepBioisostere model, and the insertion fragments are attached following the selected attachment orientations. For more details about the generation process, refer to the Supplementary Information.

Data Availability

The code for processing data from the ChEMBL database is available on GitHub: <https://github.com/Hwoo-Kim/DeepBioisostere.git>

Code Availability

The code for training DeepBioisostere, sampling molecules, and evaluating the generated structures is available on GitHub: <https://github.com/Hwoo-Kim/DeepBioisostere.git>

References

- [1] Di, L., Kerns, E.H.: Chapter 1 - introduction. In: Di, L., Kerns, E.H. (eds.) *Drug-Like Properties (Second Edition)*, Second edition edn., pp. 1–3. Academic Press, Boston (2016). <https://doi.org/10.1016/B978-0-12-801076-1.00001-0> . <https://www.sciencedirect.com/science/article/pii/B9780128010761000010>
- [2] Langdon, S.R., Ertl, P., Brown, N.: Bioisosteric replacement and scaffold hopping in lead generation and optimization. *Mol. Inf.* **29**(5), 366–385 (2010) <https://doi.org/10.1002/minf.201000019>
- [3] Dick, A., Cocklin, S.: Bioisosteric replacement as a tool in anti-HIV drug design. *Pharmaceuticals* **13**(3), 36 (2020) <https://doi.org/10.3390/ph13030036>
- [4] Cao, X., Yang, H., Liu, C., Zhang, R., Maienfisch, P., Xu, X.: Bioisosterism and scaffold hopping in modern nematicide research. *J. Agric. Food Chem.* **70**(36), 11042–11055 (2022) <https://doi.org/10.1021/acs.jafc.2c00785>
- [5] Zou, Y., Liu, L., Liu, J., Liu, G.: *Bioisosteres in drug discovery: focus on tetrazole*. Future Science (2020)
- [6] Malik, M.A., Wani, M.Y., Al-Thabaiti, S.A., Shiekh, R.A.: Tetrazoles as carboxylic acid isosteres: chemistry and biology. *J Incl Phenom Macrocycl Chem* **78**(1-4), 15–37 (2013) <https://doi.org/10.1007/s10847-013-0334-x>
- [7] Subbaiah, M.A.M., Meanwell, N.A.: Bioisosteres of the phenyl ring: Recent strategic applications in lead optimization and drug design. *Journal of Medicinal Chemistry* **64**(19), 14046–14128 (2021) <https://doi.org/10.1021/acs.jmedchem.1c01215>
- [8] Patani, G.A., LaVoie, E.J.: Bioisosterism: a rational approach in drug design. *Chemical reviews* **96**(8), 3147–3176 (1996)
- [9] Ertl, P.: In silico identification of bioisosteric functional groups. *Current opinion in drug discovery & development* **10**(3), 281–288 (2007)
- [10] Kumari, S., Carmona, A.V., Tiwari, A.K., Trippier, P.C.: Amide bond bioisosteres: Strategies, synthesis, and successes. *Journal of medicinal chemistry* **63**(21), 12290–12358 (2020)
- [11] Seddon, M.P., Cosgrove, D.A., Gillet, V.J.: Bioisosteric replacements extracted

- from high-quality structures in the protein databank. *ChemMedChem* **13**(6), 607–613 (2018)
- [12] Papadatos, G., Brown, N.: In silico applications of bioisosterism in contemporary medicinal chemistry practice. *WIREs Computational Molecular Science* **3**(4), 339–354 (2013) <https://doi.org/10.1002/wcms.1148>
- [13] Wirth, M., Zoete, V., Michielin, O., Sauer, W.H.: Swissbioisostere: a database of molecular replacements for ligand design. *Nucleic acids research* **41**(D1), 1137–1143 (2013)
- [14] Cai, C., Gong, J., Liu, X., Gao, D., Li, H.: Molecular similarity: Methods and performance. *Chin. J. Chem.* **31**(9), 1123–1132 (2013) <https://doi.org/10.1002/cjoc.201300390>
- [15] Ertl, P.: World wide web-based system for the calculation of substituent parameters and substituent similarity searches. *Journal of Molecular Graphics and Modelling* **16**(1), 11–13 (1998)
- [16] Schuffenhauer, A., Gillet, V.J., Willett, P.: Similarity searching in files of three-dimensional chemical structures: analysis of the BIOSTER database using two-dimensional fingerprints and molecular field descriptors. *J. Chem. Inf. Comput. Sci.* **40**(2), 295–307 (1999) <https://doi.org/10.1021/ci990263g>
- [17] Thormann, M., Klamt, A., Hornig, M., Almstetter, M.: Cosmosim: Bioisosteric similarity based on cosmo-rs σ profiles. *Journal of Chemical Information and Modeling* **46**(3), 1040–1053 (2006) <https://doi.org/10.1021/ci050464m>
- [18] Devereux, M., Popelier, P.L.A., McLay, I.M.: Quantum isostere database: A web-based tool using quantum chemical topology to predict bioisosteric replacements for drug design. *J. Chem. Inf. Model.* **49**(6), 1497–1513 (2009) <https://doi.org/10.1021/ci900085d>
- [19] Wagener, M., Lommerse, J.P.M.: The quest for bioisosteric replacements. *J. Chem. Inf. Model.* **46**(2), 677–685 (2006) <https://doi.org/10.1021/ci0503964>
- [20] Wood, D.J., Vlieg, J.d., Wagener, M., Ritschel, T.: Pharmacophore fingerprint-based approach to binding site subpocket similarity and its application to bioisostere replacement. *Journal of chemical information and modeling* **52**(8), 2031–2043 (2012)
- [21] Krier, M., Hutter, M.C.: Bioisosteric similarity of molecules based on structural alignment and observed chemical replacements in drugs. *Journal of chemical information and modeling* **49**(5), 1280–1297 (2009)
- [22] Ujváry, I.: Extended summary: Bioster—a database of structurally analogous compounds. *Pesticide Science* **51**(1), 92–95 (1997)

- [23] Desaphy, J., Rognan, D.: sc-PDB-frag: A database of protein–ligand interaction patterns for bioisosteric replacements. *J. Chem. Inf. Model.* **54**(7), 1908–1918 (2014) <https://doi.org/10.1021/ci500282c>
- [24] Lešnik, S., Škrlić, B., Eržen, N., Bren, U., Gobec, S., Konc, J., Janežič, D.: Bober: web interface to the base of bioisosterically exchangeable replacements. *Journal of Cheminformatics* **9**(1), 1–8 (2017)
- [25] Griffen, E., Leach, A.G., Robb, G.R., Warner, D.J.: Matched molecular pairs as a medicinal chemistry tool. *J. Med. Chem.* **54**(22), 7739–7750 (2011) <https://doi.org/10.1021/jm200452d>
- [26] Mendez, D., Gaulton, A., Bento, A.P., Chambers, J., De Veij, M., Félix, E., Magariños, M.P., Mosquera, J.F., Mutowo, P., Nowotka, M., *et al.*: ChEMBL: towards direct deposition of bioassay data. *Nucleic acids research* **47**(D1), 930–940 (2019)
- [27] Timmerman, H., Todeschini, R., Consonni, V., Mannhold, R., Kubinyi, H.: *Handbook of molecular descriptors*. Weinheim: Wiley-VCH (2002)
- [28] Ertl, P.: Identification of bioisosteric substituents by a deep neural network. *Journal of Chemical Information and Modeling* **60**(7), 3369–3375 (2020) <https://doi.org/10.1021/acs.jcim.0c00290>
- [29] Shan, J., Ji, C.: Molopt: a web server for drug design using bioisosteric transformation. *Current computer-aided drug design* **16**(4), 460–466 (2020)
- [30] Jin, W., Barzilay, R., Jaakkola, T.: Multi-objective molecule generation using interpretable substructures. In: *International Conference on Machine Learning*, pp. 4849–4859 (2020). PMLR
- [31] Fu, T., Xiao, C., Li, X., Glass, L.M., Sun, J.: Mimosa: Multi-constraint molecule sampling for molecule optimization. In: *Proceedings of the AAAI Conference on Artificial Intelligence*, vol. 35, pp. 125–133 (2021)
- [32] Loeffler, H.H., He, J., Tibo, A., Janet, J.P., Voronov, A., Mervin, L.H., Engkvist, O.: Reinvent 4: modern ai-driven generative molecule design. *Journal of Cheminformatics* **16**(1), 20 (2024)
- [33] He, J., You, H., Sandström, E., Nittinger, E., Bjerrum, E.J., Tyrchan, C., Czechtizky, W., Engkvist, O.: Molecular optimization by capturing chemist’s intuition using deep neural networks. *Journal of Cheminformatics* **13**(1) (2021) <https://doi.org/10.1186/s13321-021-00497-0>
- [34] He, J., Nittinger, E., Tyrchan, C., Czechtizky, W., Patronov, A., Bjerrum, E.J., Engkvist, O.: Transformer-based molecular optimization beyond matched molecular pairs. *Journal of Cheminformatics* **14**(1) (2022) <https://doi.org/10.1186/>

- [35] Yang, L., Jin, C., Yang, G., Bing, Z., Huang, L., Niu, Y., Yang, L.: Transformer-based deep learning method for optimizing ADMET properties of lead compounds. *Physical Chemistry Chemical Physics* **25**(3), 2377–2385 (2023) <https://doi.org/10.1039/d2cp05332b>
- [36] Jin, W., Barzilay, R., Jaakkola, T.: Hierarchical graph-to-graph translation for molecules. arXiv preprint arXiv:1907.11223 (2019)
- [37] Jin, W., Barzilay, R., Jaakkola, T.: Hierarchical generation of molecular graphs using structural motifs. In: *International Conference on Machine Learning*, pp. 4839–4848 (2020). PMLR
- [38] Chen, Z., Min, M.R., Parthasarathy, S., Ning, X.: A deep generative model for molecule optimization via one fragment modification. *Nature Machine Intelligence* **3**(12), 1040–1049 (2021) <https://doi.org/10.1038/s42256-021-00410-2>
- [39] Zheng, S., Lei, Z., Ai, H., Chen, H., Deng, D., Yang, Y.: Deep scaffold hopping with multimodal transformer neural networks. *Journal of Cheminformatics* **13**(1) (2021) <https://doi.org/10.1186/s13321-021-00565-5>
- [40] Hu, C., Li, S., Yang, C., Chen, J., Xiong, Y., Fan, G., Liu, H., Hong, L.: Scaffoldgvae: scaffold generation and hopping of drug molecules via a variational autoencoder based on multi-view graph neural networks. *Journal of Cheminformatics* **15**(1), 91 (2023) <https://doi.org/10.1186/s13321-023-00766-0>
- [41] Maziarka, L., Pocha, A., Kaczmarczyk, J., Rataj, K., Danel, T., Warchoł, M.: Mol-cyclegan: a generative model for molecular optimization. *Journal of Cheminformatics* **12**(1), 2 (2020)
- [42] Degen, J., Wegscheid-Gerlach, C., Zaliani, A., Rarey, M.: On the art of compiling and using 'drug-like' chemical fragment spaces. *ChemMedChem* **3**(10), 1503–1507 (2008) <https://doi.org/10.1002/cmdc.200800178>
- [43] Zhou, Z., Kearnes, S., Li, L., Zare, R.N., Riley, P.: Optimization of molecules via deep reinforcement learning. *Scientific reports* **9**(1), 10752 (2019)
- [44] Wildman, S.A., Crippen, G.M.: Prediction of physicochemical parameters by atomic contributions. *Journal of chemical information and computer sciences* **39**(5), 868–873 (1999)
- [45] Bickerton, G.R., Paolini, G.V., Besnard, J., Muresan, S., Hopkins, A.L.: Quantifying the chemical beauty of drugs. *Nature chemistry* **4**(2), 90–98 (2012)
- [46] Ertl, P., Schuffenhauer, A.: Estimation of synthetic accessibility score of drug-like molecules based on molecular complexity and fragment contributions. *Journal of*

- cheminformatics **1**, 1–11 (2009)
- [47] Walters, W.P.: Virtual chemical libraries: miniperspective. *Journal of medicinal chemistry* **62**(3), 1116–1124 (2018)
- [48] Gao, W., Coley, C.W.: The synthesizability of molecules proposed by generative models. *Journal of chemical information and modeling* **60**(12), 5714–5723 (2020)
- [49] Lassalas, P., Gay, B., Lasfargeas, C., James, M.J., Tran, V., Vijayendran, K.G., Brunden, K.R., Kozlowski, M.C., Thomas, C.J., Smith III, A.B., *et al.*: Structure property relationships of carboxylic acid isosteres. *Journal of medicinal chemistry* **59**(7), 3183–3203 (2016)
- [50] Peng, X., Luo, S., Guan, J., Xie, Q., Peng, J., Ma, J.: Pocket2mol: Efficient molecular sampling based on 3d protein pockets. In: *International Conference on Machine Learning*, pp. 17644–17655 (2022). PMLR
- [51] Zhung, W., Kim, H., Kim, W.Y.: 3d molecular generative framework for interaction-guided drug design. *Nature Communications* **15**(1), 2688 (2024)
- [52] Guan, J., Qian, W.W., Peng, X., Su, Y., Peng, J., Ma, J.: 3d equivariant diffusion for target-aware molecule generation and affinity prediction. In: *International Conference on Learning Representations* (2023)
- [53] Guan, J., Zhou, X., Yang, Y., Bao, Y., Peng, J., Ma, J., Liu, Q., Wang, L., Gu, Q.: Decompdiff: diffusion models with decomposed priors for structure-based drug design. In: *Proceedings of the 40th International Conference on Machine Learning*, pp. 11827–11846 (2023)
- [54] Landrum, G.: RDKit: open-source cheminformatics. <http://www.rdkit.org>
- [55] Chung, J., Gulcehre, C., Cho, K., Bengio, Y.: Empirical Evaluation of Gated Recurrent Neural Networks on Sequence Modeling. *arXiv* (2014). <https://doi.org/10.48550/ARXIV.1412.3555> . <https://arxiv.org/abs/1412.3555>
- [56] Seo, S., Lim, J., Kim, W.Y.: Molecular generative model via retrosynthetically prepared chemical building block assembly. *Advanced Science* **10**(8), 2206674 (2023)

Acknowledgments

This work was supported by Basic Science Research Programs through the National Research Foundation of Korea, funded by the Ministry of Science and ICT (Grant Nos. RS-2023-NR077040, RS-2022-NR068758) and by the Ministry of Health and Welfare (Grant No. RS-2024-00512498) to H.K., S.M., W.Z., S.K., and W.Y.K.

Author contributions

H.K. and S.M. equally contributed to this work. H.K. and S.M. designed the methodology and carried out the experiments. H.K., S.M., W.Z., and S.K. designed the experiments and analyzed the results. All authors wrote the manuscript together, and W.Y.K. supervised the project.

Competing interests

The authors declare no competing interests.

Electronic Supplementary Information for: Autonomous Bioisosteric Replacement for Multi-Property Optimization in Drug Design

Hyeongwoo Kim,^{a‡} Seokhyun Moon^{a‡}, Wonho Zhung,^a Shinwoo Kim,^a
Jaechang Lim^b and Woo Youn Kim^{*abc}

^aDepartment of Chemistry, KAIST, 291, Daehak-ro, Yuseong-gu, Daejeon, 34141, Republic of Korea.

^bHITS Inc., 124, Teheran-ro, Gangnam-gu, 06234, Seoul, Republic of Korea.

^cGraduate School of Data Science, KAIST, 291, Daehak-ro, Yuseong-gu, Daejeon, 34141, Republic of Korea.

*Corresponding author; E-mail: wooyoun@kaist.ac.kr.

‡These authors contributed equally to this work.

Contents

1	Architecture details	2
1.1	Node and edge features	2
1.2	Embedding of complete molecules and molecular fragments	2
2	Training details	3
2.1	Post-processing the constructed MMP dataset for training	3
2.2	Training with negative sampling strategy	3
2.3	Hyper-parameters for training DeepBioisostere	4
3	Generation details	5
3.1	Pre-processing for generation	5
3.2	Optimization process with DeepBioisostere	5
4	Dataset statistics	6
4.1	Property distributions of the training dataset	6
4.2	Statistics of the fragment library	6
5	Additional results and discussions	9
5.1	Ablation study on architecture design	9
5.2	Analysis with additional test sets	10
5.3	More statistical analysis on multi-property control scenarios	12
6	Generated molecule examples and analysis	13
6.1	Property distributions of multi-property controlled molecules	13
6.2	More examples of bioisosteres for an uncommon fragment	14
7	Details on the <i>in silico</i> hit-to-lead workflow	15
7.1	Used structure-based 3D molecular generative models	15
7.2	Target selection criteria and statistics of generated molecules	15
7.3	Additional results	16

1 Architecture details

1.1 Node and edge features

A molecule and molecular fragments are represented as nodes and edges corresponding to atoms and bonds, respectively. Supplementary Table 1 summarizes the atom and edge features used in this work, $\hat{\mathbf{a}}_i \in \mathbb{R}^{F_a}$ and $\hat{\mathbf{e}}_i \in \mathbb{R}^{F_e}$. A feature with more than two available options is represented in a one-hot vector corresponding to its category, while a feature with only two options (bool type) is encoded into a bit vector. Hydrogen atoms are represented implicitly by the feature of ‘Num hydrogens’. Ring structures, including aromatic rings, are crucial information in drug discovery, so we included both features and represented them as one-hot vectors.

Node feature	Available options
Period	1, 2, 3, 4, 5, 6, <i>else</i>
Group	1, 2, 13, 14, 15, 16, 17, 18, <i>else</i>
Degree	0, 1, 2, 3, 4, 5, 6, <i>else</i>
Formal charge	-2, -1, 0, 1, 2, <i>else</i>
Num hydrogens	0, 1, 2, 3, 4, <i>else</i>
Chirality ^a	cw, ccw, unspecified, <i>else</i>
Hybridization	<i>s</i> , <i>sp</i> , <i>sp</i> ² , <i>sp</i> ³ , <i>sp</i> ³ <i>d</i> , <i>sp</i> ³ <i>d</i> ² , <i>else</i>
Aromaticity (bit)	<i>true</i> , <i>false</i>
Ring member (bit)	<i>true</i> , <i>false</i>
BRICS type ^b	1, 2, 3, 4, 5, 6, 7, 8, 9, 10, 11, 12, 13, 14, 15, 16, 17
Edge feature	Available options
Bond order	single, double, triple, aromatic
Stereochemistry	Z, E, cis, trans, any, none
Conjugated (bit)	<i>true</i> , <i>false</i>
BRICS-allowed ^c (bit)	<i>true</i> , <i>false</i>

^a cw: clockwise (R configuration). ccw: Counter-clockwise (S configuration).

^b The BRICS type is assigned only for dummy atoms to represent the BRICS types of broken bonds. Refer to supplementary section 1.2.

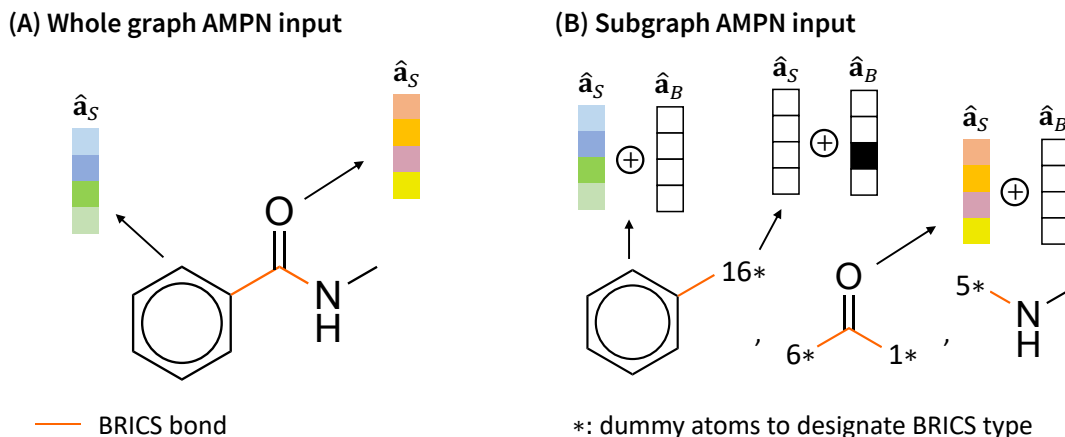
^c Representing whether a particular bond can be broken based on the BRICS rules.

Supplementary Table 1: Atom and edge features and their available items used in this work. All information is encoded into either one-hot or bit vectors to be concatenated into node and edge feature vectors.

1.2 Embedding of complete molecules and molecular fragments

One of the key characteristics of DeepBiosostere is a hierarchical architecture that handles a molecule at the levels of both atom and fragment. For embedding a single molecule, it is first analyzed by the BRICS rules to yield irreducible fragments. Afterward, a whole graph AMPN runs on the original molecular structure, while a subgraph AMPN operates on each internal fragment. The hidden vectors from each AMPN network are then aggregated into the fragment level and concatenated to fragment embedding vectors; $\mathbf{f}_n^0 = [\mathbf{w}_n \parallel \mathbf{s}_n]$. We note that input for subgraph AMPN comprises molecular fragments with dummy atoms to designate allowed attachment sites. We defined the atom feature vector of the dummy atoms to carry information only about the BRICS types and no information about other features in Supplementary Table 1. To match the dimension, a zero vector is concatenated into the feature vectors of non-dummy atoms. The resulting feature dimensions of a node and edge are $F_a = 66$ and $F_e = 12$, respectively. An example of this process is illustrated in Supplementary Fig. 1.

As a complete molecule is embedded by the embedding networks of DeepBiosostere, molecular fragments from the fragment library are embedded to be used as inputs for the insertion fragment selection module, θ_I . The nodes of a molecular fragment are embedded by whole graph and subgraph AMPN networks and



Supplementary Figure 1: $\hat{\mathbf{a}}_S$ is a concatenation of one-hot vectors to represent structural atom features, and $\hat{\mathbf{a}}_B$ is a one-hot vector to designate the BRICS type of a dummy atom. The numbers in front of the dummy atom symbol, *, indicate the corresponding BRICS types of broken attachment sites.

aggregated into a single embedding vector for that single fragment, the same way where the fragment-level embeddings of a complete molecule are obtained. The AMPN networks for a molecular fragment share their parameters with the AMPN networks for embedding a complete molecule. In this manner, molecular fragments are embedded without any bias on whether they come from a molecule or a fragment library. This implementation enables the AMPN networks to encounter diverse molecular fragments so that they can behave stably when a rare fragment takes part.

2 Training details

2.1 Post-processing the constructed MMP dataset for training

DeepBioisostere consists of three main modules, which are trained simultaneously with the training dataset we constructed. Each data point comprises an MMP for which two chemical modifications can be identified in opposite directions. For the respective modification, the differences in the molecular properties are used to construct the property control condition, *DeepICL*. Hence, two modifications with opposite directions and property control conditions are defined from each MMP data point. Removal and insertion fragments in the retrieved modifications are gathered to organize a fragment library to be used in the training and sampling processes.

2.2 Training with negative sampling strategy

In this work, we formulated three loss functions for the three main modules in the form of binary cross-entropy loss: \mathcal{L}_{remove} , \mathcal{L}_{insert} , and \mathcal{L}_{attach} . With a typical strategy for multi-class classification problems, a model is trained to predict an extremely sparse vector for each training data point—only a single 1 among about 200,000 zeros. Adopting the embedding vectors of the entire fragment library is a possible option to resolve this sparsity problem, but it might cause a substantial inefficiency in the training phase to evaluate tens of thousands of fragments for every data point. Thus, we implemented a negative sampling inspired by Seo et al., where only tens of negative answers are randomly sampled from a pre-defined fragment library and used to calculate the training loss for every single data point and epoch.[1] We implemented different negative sampling methods for each main module since their expected functions are subtly different; it is enough for the θ_R and θ_A modules to prioritize an answer over a few other options originating from the original molecule, but the θ_I module should find out a proper fragment from a large number of external options from a pre-defined fragment library.

In the case of the θ_I module, for insertion fragment selection, we employ a random sampling to choose a few negative samples (the quantity as a hyperparameter was set to 20 in this work) from the fragment library except for a ground-truth fragment for each data point, and the selected fragments are treated as them as negative answers. We note that only fragments possessing the same number of attachment points as the ground truth and conforming to the BRICS rules for attachment with the remaining fragments are exclusively considered. In the cases of the θ_R and θ_A modules, responsible for removal fragment and attachment orientation selection, we designate all non-answer options from the original molecule as negative samples. Particularly, the internal fragments with no more than 12 atoms in the original molecule and different combinations of attachments are regarded as negative samples. We sampled negative answers with these intricate criteria since, in the sampling phase, we would allow the DeepBioisostere model to choose an option from the available choices that adhered to the specified criteria for each module.

We noticed that the frequency of removal and insertion fragments is highly imbalanced; that is, the times each fragment appears as a ground truth are different. Let’s suppose fragments A and B appear 10,000 and 1 times as positive samples, respectively, and 1 time as negative samples for insertion fragment selection. In this training scenario, a model is vulnerable to being trained to prefer fragment A regardless of the situation it encounters. Thus, overlooking this imbalance problem might lead to a trained model that depends solely on the frequency data for crucial decisions. For this purpose, we adopted two training strategies — reflecting the frequency information on the negative sampling for the insertion fragment and employing a weighted sampler to resolve the imbalance problem in the removal fragment. The negative samples for insertion fragment selection are sampled with a probability rate weakly proportional to the fragment frequency. Formally,

$$p(f_{neg}^I = f_i) \propto \text{freq}_{I,i}^{\alpha_1}, \quad (1)$$

where f_i is a fragment in the pre-defined fragment library, $\text{freq}_{I,i}$ is the occurrence of f_i in the fragment library, and α_1 is a hyper-parameter to control the dependency of negative sampling on the frequency data. The hyper-parameter α_1 can take a value in the range of $[0,1]$. Here, 0 designates a sampling from the uniform distribution, while 1 corresponds to a sampling with probabilities linearly proportional to the frequencies.

The imbalance problem in removal fragments is handled by a weighted sampling strategy. Different from the insertion fragment selection, we utilize substructures of the original molecule other than the ground truth as negative samples. This implies that we cannot adopt an external fragment as a negative sample for a certain data point. Hence, resolving the imbalance problem in removal fragments should work at the level of training data sampling. We employ WeightedRandomSampler implemented in PyTorch that generates mini-batches by sampling a number of MMP data points from the training dataset with given weighted probabilities.[2] We introduce an additional hyper-parameter α_2 to control the dependency of the training data sampling on the removal fragment frequencies. The probability of each data point to be sampled is as follows:

$$p(\text{data} = \text{data}_i) \propto \text{freq}_{R,i}^{\alpha_2}, \quad (2)$$

where data_i is a data point in the training dataset, $\text{freq}_{R,i}$ is the occurrence of the removal fragment of data_i in the training dataset, and α_2 is a hyper-parameter to control the dependency of the weighted sampler on the frequencies. The hyper-parameter α_2 can take a value in the range of $[-1,0]$. In this context, -1 compels the model to encounter all removal fragments an equal number of times, while 0 allows all training data to be sampled with an equal probability, leading to an unbalanced sampling in terms of removal fragments.

2.3 Hyper-parameters for training DeepBioisostere

The hyper-parameter setting for the reported DeepBioisostere model is summarized in Supplementary Table 2. The model hyper-parameters are used mainly for the embedding layers of AMPN and FMPN and the three main selection modules. Many training hyper-parameters are ones for the ReduceLROnPlateau learning rate scheduler implemented in the PyTorch package that gradually reduces the learning rate for convergence stability. [2] The training hyper-parameters α_1 and α_2 are responsible for controlling the dependency of the DeepBioisostere model on fragment frequencies in the fragment library and MMP dataset, respectively. Since the occurrence of removal and insertion fragments in the datasets are highly imbalanced, they are very crucial to finding novel bioisosteres.

Model param.	Descriptions	Values
F_a^h	node hidden dimension	256
F_e^h	edge hidden dimension	256
$N_{AMPN_{whole}}$	num layers of whole-graph AMPN network	4
$N_{AMPN_{sub}}$	num layers of subgraph AMPN network	4
N_{FMPN}	num layers of FMPN network	2
N_{θ_R}	num layers of removal fragment selection module, θ_R	3
N_{θ_I}	num layers of insertion fragment selection module, θ_I	3
$N_{\theta_{pocket2mol}}$	num layers of attachment orientation selection module, θ_A	3
Training param.	Descriptions	Values
B_d	batch size for data points	512
B_f	batch size for fragment library embedding	512
lr	initial learning rate	2×10^{-4}
lr _{min}	minimum learning rate ^a	1×10^{-7}
lr _{factor}	lr decaying factor ^a	0.5
lr _{patience}	lr decay tolerance epochs ^a	10
lr _{threshold}	threshold for measuring the new optimum based on loss decrease ^a	1×10^{-3}
p _{dropout}	dropout rate	0.2
α_1	exponent to the negative sampling rate of insertion fragment ^b	0.5
α_2	exponent to the weighted random sampler for removal fragment ^b	-0.5
N_{neg}	number of negative samples to train θ_I module	20

^a Parameters for the ReduceLROnPlateau scheduler implemented in PyTorch. [2]

^b Please refer to Eq. (1) and Eq. (2) for more detailed definitions.

Supplementary Table 2: Descriptions of the hyper-parameters and their values used in this work.

3 Generation details

3.1 Pre-processing for generation

DeepBioisostere performs property optimization with two inputs: a molecule to be modified, M , and a property control condition, C . First, the molecule is pre-processed based on the BRICS rules before being queried to the DeepBioisostere model. All BRICS bonds inside the molecule are identified so that its fragment-level graph representation is obtained. Then, substructures of the fragment-level graph are enumerated as potential removal fragments. Here, only a substructure that meets two strict criteria on its size is identified as an allowed removal fragment: 1) the number of heavy atoms should be less than or equal to 12, and 2) the number of heavy atoms should be less than or equal to the total number of atoms of remaining fragments. All the allowed fragments are to be examined by the removal fragment selection module θ_R in the later step.

3.2 Optimization process with DeepBioisostere

After pre-processing, the DeepBioisostere model encodes the given molecule along with the property control condition C into fragment-level embedding vectors. An embedding vector of each allowed fragment, \mathbf{h}_f , is obtained by summing the embedding vectors of internal irreducible fragments, following the equation (8) in the main text. Then, the removal fragment selection module θ_R utilizes the embedding vectors $\{\mathbf{h}_f\}$ to examine the likelihood of each allowed fragment as the equation (9) in the main text. From the multinomial probability distribution of the allowed fragments, the DeepBioisostere model performs random sampling until a pre-defined number of samples are obtained. We note that this process allows duplication so that the numbers of sampled removal fragments follow the multinomial distribution estimated by the model.

The DeepBioisostere model then explores the fragment library to find suitable insertion fragments for each removal fragment to achieve the property control condition. For each removal fragment, insertion

fragments that satisfy the following two criteria are evaluated by the model: 1) the number of attachment sites, or fragmented sites, should be the same as that of the removal fragment, and 2) the BRICS types of the sites are allowed to be attached to the remaining fragments. All the passed fragments are evaluated for their likelihood by the insertion fragment selection module θ_I as the equation (10), and highly ranked insertion fragments are greedily selected. It means that for each removal fragment, top-k insertion fragments are chosen according to the number of samples determined in the previous step. This greedy selection is possible since DeepBioisostere is a generative model that estimates the explicit likelihood of a generated sample.

Lastly, DeepBioisostere determines the attachment orientations of the selected insertion fragments. This step is performed as explained in the main text; only BRICS-allowed combinations are prioritized by the DeepBioisostere model. For each removal and insertion fragment pair, the top-1 attachment orientation is selected as an assembly template to which the DeepBioisostere model refers to build a final molecular structure.

4 Dataset statistics

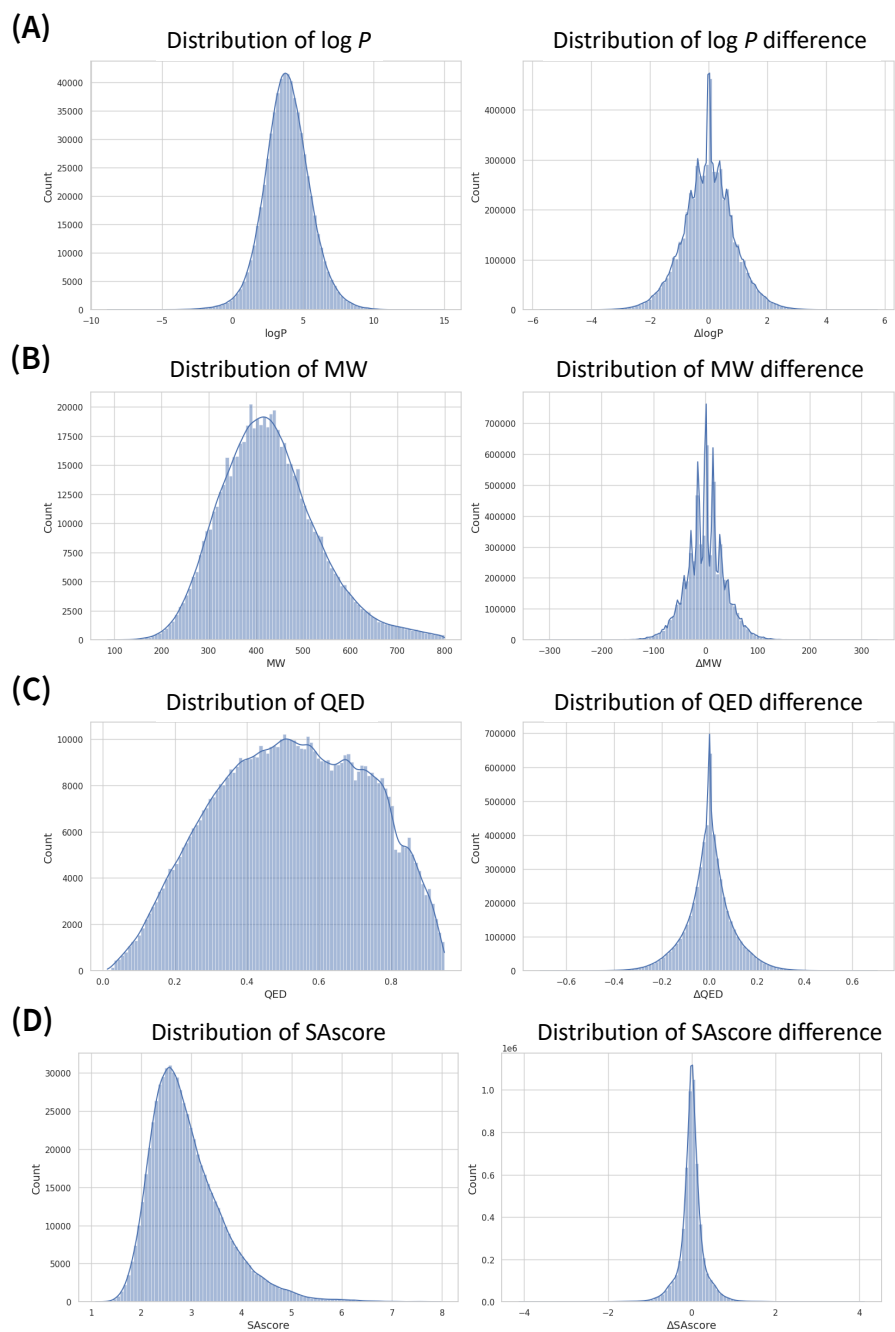
4.1 Property distributions of the training dataset

For a more reliable estimation of the DeepBioisostere model’s performance on multi-property control tasks (Section 2.2 in the main text), we present distributions of molecular properties and property deviations for MMPs. From the training dataset, we utilized all resulting molecules to illustrate the former distribution, while for the latter, all MMPs were employed. Fig. 2 shows the distributions for four properties considered in our property control tasks: the logarithm of the octanol-water partition coefficient ($\log P$), molecular weight (MW), quantitative estimate of drug-likeness (QED), and synthetic accessibility score (SAscore).

Notably, the QED difference distribution in Fig. 2(C) shows that increasing QED by 0.1 and 0.2 corresponds to 1.03 and 2.05 standard deviations, respectively - indicating that achieving a 0.2 QED gain is more challenging than increasing it by 0.1. For SAscore (Fig. 2(D)), our property control objectives include a 0.5 decrease (1.67 STD) and an even more demanding 1.0 decrease (3.32 STD). Yet, fewer than 0.05% of pairs in the training dataset exhibit SAscore differences above 1.0. Due to this statistical nature, QED or SAscore-control tasks become significantly more challenging.

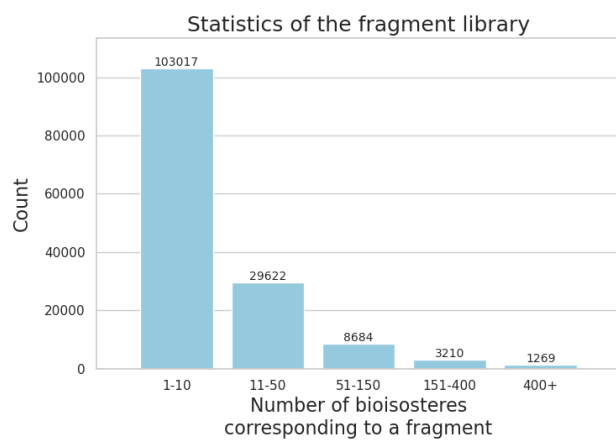
4.2 Statistics of the fragment library

We conducted a statistical analysis of the number of bioisosteres corresponding to a fragment to illustrate the potential challenges that database mining approaches might face in the discovery of novel bioisosteres. Since our dataset only consists of MMPs, we first counted the number of bioisosteres for each fragment in our fragment library and then constructed a distribution based on these counts. Fig. 3(A) illustrates the resulting distribution, which includes 145,959 fragments from our library. As noted in the main text, a significant portion of the fragments, over 100,000, has ten or fewer bioisosteres, while only 1,269 fragments have 400 or more bioisosteres. Furthermore, Fig. 3(B) highlights 10 fragments with the highest number of bioisosteres. It comes with no surprise that benzene derivatives or methoxy groups, which are among the most common moieties, are found in these fragments, in contrast to the triazolo pyridazine moiety mentioned in the main text.

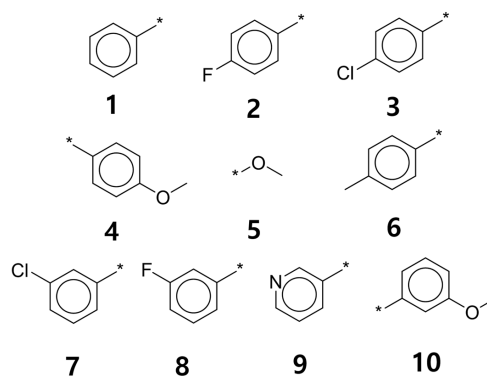


Supplementary Figure 2: Distributions of $\log P$, MW, QED, and SAScore in our MMP database. For all properties, the first and second columns represent the molecule's property and MMP's property deviation distributions, respectively.

(A)



(B)

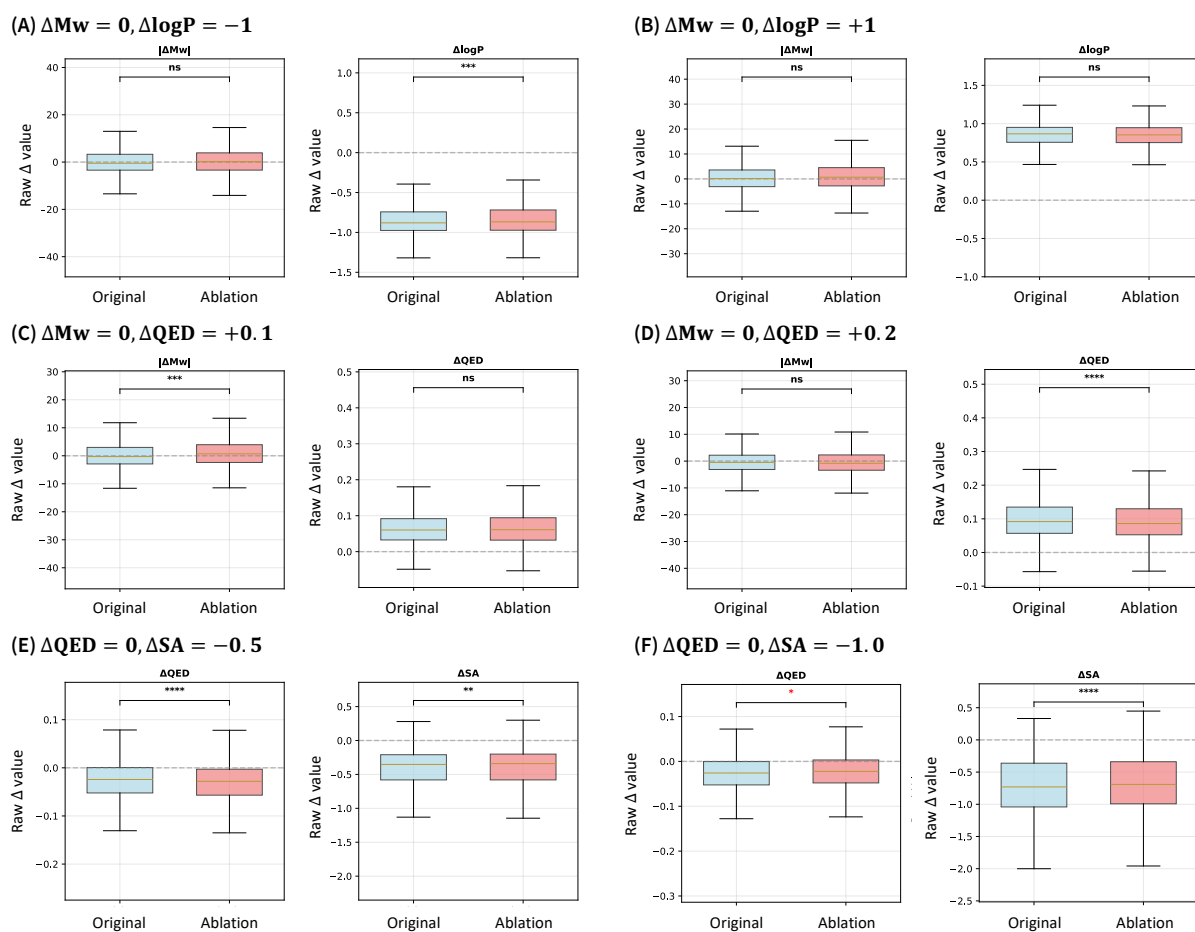


Supplementary Figure 3: Statistical analysis of the fragment library we constructed. (A) Statistics of the numbers of bioisosteres for each fragment in our fragment library. (B) The top 10 molecules that have the top 10 largest numbers of bioisosteres based on our MMP database.

5 Additional results and discussions

5.1 Ablation study on architecture design

We performed an ablation study on the architectural design of DeepBioisostere for the multi-property control task described in Section 2.2. We trained a DeepBioisostere model ablated with the subgraph AMPN during the original molecule embedding procedure; in this model the subgraph AMPN is not shared across the molecule and fragment library embeddings, but only used for the fragment library. In the original DeepBioisostere model, outputs from the whole graph AMPN and subgraph AMPN are concatenated and used as an initial hidden vector for the FMPN. However, the subgraph AMPN is not used for original molecule embedding in the ablated model, we added a linear layer between AMPN and FMPN to upscale the whole graph AMPN outputs to fit the FMPN dimension, ensuring the ablated model to have equivalent model parameter size.



Supplementary Figure 4: Paired t-test results to compare multi-property control performances; ns $P > 0.1$, $*P < 0.1$, $**P < 0.05$, $***P < 0.01$, and $****P < 0.001$. Black stars designate the original model statistically achieves higher performance, and red ones mean the ablated model exhibits better results. Used input property control conditions are shown in sub-titles. (A,B) Scenario where MW and $\log P$ are modulated simultaneously. (C,D) Scenario where MW and QED are modulated simultaneously. (E,F) Scenario where QED and SA are modulated simultaneously.

As in Section 2.2, we applied the ablated model to the same test molecules with the same property control conditions, generating distinct sets of modified molecular structures. We then applied paired t-test that

examines the property improvements or maintenance for each original molecule. Thus, the hypothesis to be examined is that, for each given molecule, DeepBioisostere model is better at improving or maintaining target property than the ablated model. The results in Fig. 4 show that the DeepBioisostere model demonstrates superior performance compared to the ablated model in most conditioning scenarios. One exception is when property condition of $\Delta\text{QED} = 0$ and $\Delta\text{SA} = -1.0$ was used (Fig. 4(F)), where the ablated model exhibited better QED maintenance with weak significance level ($P = 8.23 * 10^{-2}$) but the DeepBioisostere model improved SA with much strong significance ($P = 4.42 * 10^{-9}$). This ablation study demonstrates that incorporating the subgraph AMPN into both the original molecule and fragment library embedding processes enables the model to better capture multiple molecular properties through fragment-level interpretation.

5.2 Analysis with additional test sets

In section 2.2 in the main manuscript, we constructed distinct test molecule sets for each property control scenario with different filtering criteria. They confined the test molecules to be appropriate for one property but not enough for the other property, intended to assume more practical situations. Thus, property control conditions were set to maintain the former and improve the latter. Here, for more statistical aspects of DeepBioisostere, we report results with randomly selected test molecules from ChEMBL that were not filtered in terms of properties that are optimized in each scenario. Still, the common filters in section 2.2 were applied: (1) a single neutral molecule, (2) molecular weight that falls within the range of 100 to 500, and (3) inclusion of at least one BRICS bond. 1,000 test molecules were randomly selected from the ChEMBL database and used as original molecules to the DeepBioisostere model. We here compare property control results for this additional test set with the results for further filtered test sets in main manuscript Table 1, section 2.2.

Table 3 shows the results for three multi-property control scenarios with the test set constructed above. In scenario 2, where MW is to be kept and QED is improved, the average ΔMW is less than 1.0, same with that in main manuscript Table 1. However, QED improvements of 0.038 and 0.060 are much smaller than those in main manuscript of 0.067 and 0.100, respectively. This is due to that test molecules in section 2.2 are ones of which QED values are less than 0.4 so that they contain more room for QED improvement. Scenario 3 is the case where a given molecule’s SAscore is improved while preventing its QED from decreasing. Compared to section 2.2 in the main manuscript, average $\Delta\text{SAscore}$ values of -0.209 and -0.285 are much weaker and average ΔQED values of -0.003 and +0.030 mean that QED was less degraded. Also in this scenario, since the given original molecules have worse SAscore for the Table 1 test set, they have more potential to be modified for better SAscore. These comparisons suggest that for the given property control condition and unsatisfying molecular structure, DeepBioisostere can find problematic sub-structures and generate appropriate bioisosteric replacements to optimize the target properties.

Scenario	Requested Optimization		Property Change	
	Property	Δ Value	Average	Std. Dev.
Scenario 1	MW	0	-0.19	12.7
	$\log P$	+1	+0.84	0.35
	MW	0	-0.18	12.5
	$\log P$	-1	-0.87	0.39
Scenario 2	MW	0	-0.20	10.6
	QED	+0.1	+0.038	0.091
	MW	0	-0.85	10.6
	QED	+0.2	+0.060	0.101
Scenario 3	QED	0	-0.003	0.099
	SAscore	-0.5	-0.209	0.262
	QED	0	+0.030	0.119
	SAscore	-1.0	-0.285	0.381

Supplementary Table 3: **Results of three multi-property control scenarios with an additional test set.** The requested optimization is the property control condition given to our model. For each scenario, we have two properties to control: Scenario 1 - modulating $\log P$ while maintaining MW. Scenario 2 - increasing QED while keeping the molecular weight. Scenario 3 - decreasing SAscore without losing QED. Δ Value is the requested property change in each property. Average and Std. Dev. designates the mean value of property change and its standard deviation, respectively.

5.3 More statistical analysis on multi-property control scenarios

Supplementary Table 4: **Paired *t*-test results for property control scenarios.** For each scenario, both the maintained and target properties are listed with their mean Δ , standard deviation, *t*-statistics, and *p*-values. Two-tailed tests were applied to the maintained properties to verify that no significant deviation occurred, while one-tailed (directional) tests were used for the target properties to confirm whether their changes were statistically consistent with the intended direction of optimization.

Scenario	Condition	Maintain	Δ (mean \pm SD)	<i>t</i> (vs 0)	<i>p</i> (vs 0)	Target	Δ (mean \pm SD)	<i>t</i> (vs 0)	<i>p</i> (vs 0)	<i>t</i> (vs target)	<i>p</i> (vs target)
1	Δ Mw 0 / Δ logP +1	Mw	0.045 \pm 6.53	0.22	0.83	logP	+0.831 \pm 0.204	128.8	< 10 ⁻⁶⁰	-26.19	2.26 \times 10 ⁻¹¹⁵
1	Δ Mw 0 / Δ logP -1	Mw	-0.27 \pm 6.19	-1.39	0.17	logP	-0.841 \pm 0.217	-122.3	< 10 ⁻⁶⁰	+23.20	1.68 \times 10 ⁻⁹⁵
2	Δ Mw 0 / Δ QED +0.10	Mw	-0.13 \pm 5.23	-0.78	0.44	QED	+0.067 \pm 0.053	39.79	5.4 \times 10 ⁻²⁰⁷	-19.43	2.20 \times 10 ⁻⁷¹
2	Δ Mw 0 / Δ QED +0.20	Mw	-0.58 \pm 5.36	-3.37	7.8 \times 10 ⁻⁴	QED	+0.100 \pm 0.062	49.98	7.6 \times 10 ⁻²⁷²	-50.34	9.29 \times 10 ⁻²⁷⁴
3	Δ QED 0 / Δ SA -0.50	QED	-0.026 \pm 0.043	-17.01	1.4 \times 10 ⁻⁵⁵	SA	-0.438 \pm 0.361	-34.14	4.2 \times 10 ⁻¹⁵⁸	+4.87	1.35 \times 10 ⁻⁶
3	Δ QED 0 / Δ SA -1.00	QED	-0.028 \pm 0.045	-17.62	6.6 \times 10 ⁻⁵⁹	SA	-0.719 \pm 0.445	-45.42	5.3 \times 10 ⁻²²³	+17.77	1.01 \times 10 ⁻⁵⁹

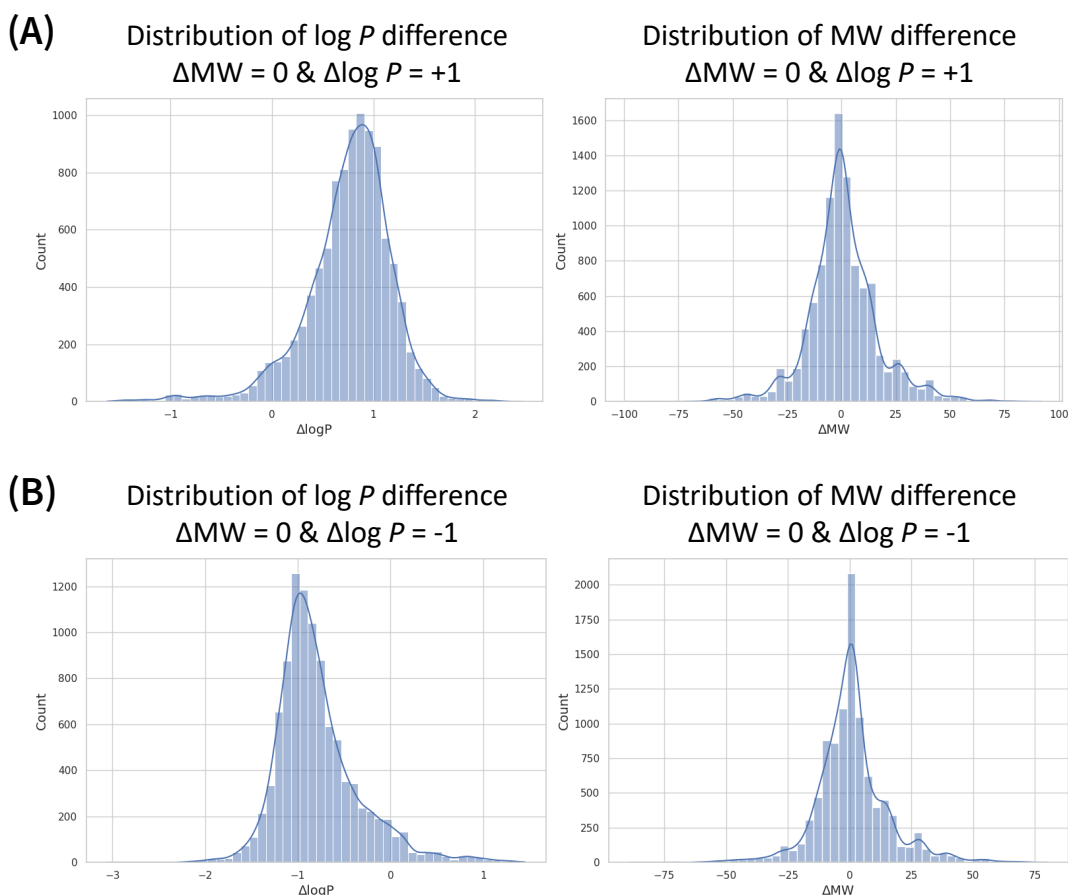
Table 4 summarizes the results of paired *t*-tests conducted for all property control scenarios and conditions described in the main manuscript. The analysis was performed using the same generated molecules presented in Table 1 of the main text, without additional sampling. To account for the stochastic nature of the generation process, each original molecule (e.g., *n* = 995, 979, 793 for Scenarios 1–3, respectively) had ten candidate structures generated, and the average property change across these variants was used as a single paired observation for the *t*-test. For each case, we evaluated whether (i) the mean change in the target property was significantly different from zero and (ii) whether it was statistically consistent with the requested numeric target. Across all scenarios, the mean shifts in the target properties were highly significant (*p* \ll 0.001), confirming that DeepBioisostere successfully modulates molecular properties in the desired direction. However, equivalence tests against the exact numeric targets ($H_0: \mu = \text{target}$) were rejected in all settings, indicating that while directional control was clearly achieved, the improvements typically reached 50–88 % of the requested magnitude. This underachievement is expected since the model performs structure-preserving molecular modifications rather than *de novo* generation, thereby being constrained by the original molecular scaffolds and interdependencies among multiple properties. Nonetheless, the results demonstrate a clear monotonic relationship between the requested target magnitude and the realized degree of property change, validating the controllability and robustness of DeepBioisostere under realistic structural constraints.

6 Generated molecule examples and analysis

6.1 Property distributions of multi-property controlled molecules

DeepBioisostere demonstrated satisfactory performance in various multi-property control tasks. Specifically, in the first scenario aimed at increasing or decreasing $\log P$ while maintaining MW , the deviations of MW between generated molecules and the originals were 6.54 and 3.41, respectively. These results suggest that most replacements suggested by our model successfully maintained the original molecules' MW since the values are smaller than the MW of a single heavy atom.

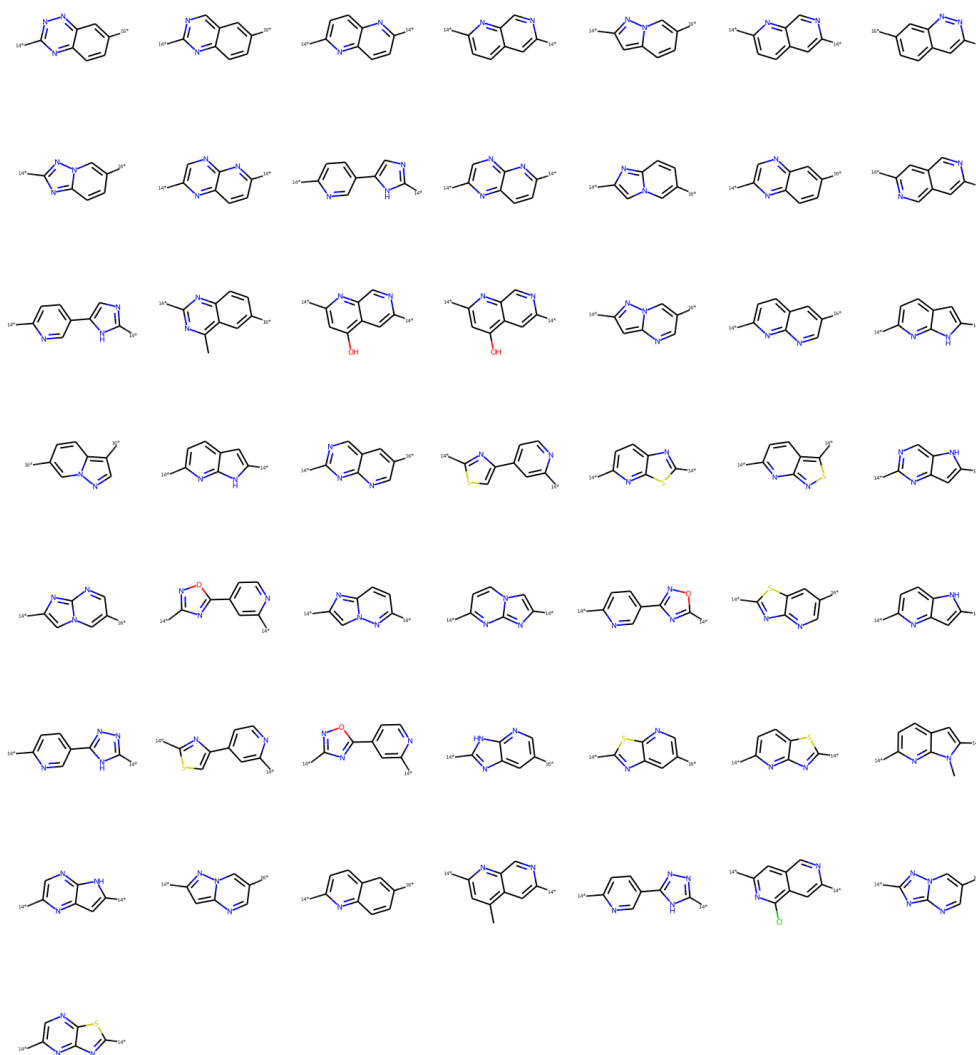
To explore this further, we performed a statistical analysis of the generated molecules, focusing on their property deviation distributions. In Fig. 5(A), where the property control condition is *increasing* $\log P$ while retaining MW , most of the molecules are distributed between -20 and 20 for the MW deviation distribution. Likewise, Fig. 5(B), with the condition changed to *decreasing* $\log P$ while retaining MW , showed similar results, indicating that the generated molecules tend to have negligible change in MW .



Supplementary Figure 5: Distributions of $\log P$ (left) and MW (right) deviations, computed from molecules generated by DeepBioisostere under the condition of increasing (A) or decreasing (B) $\log P$ by 1 while maintaining MW , alongside the original molecules.

6.2 More examples of bioisosteres for an uncommon fragment

In section 2.4 in the main text, we selectively exhibited the bioisosteres since many top-ranked fragments are structurally similar to each other. Here, for clarity, we provide 50 top-ranked fragments selected as a bioisostere for the azaindole moiety to maintain the QED value of the CHEMBL3403020 molecule. Most of them contain two aromatic rings, either fused rings or covalently bonded rings.



Supplementary Figure 6: Top 50 molecular fragments selected as the bioisosteres of an azaindole moiety in the molecule, CHEMBL3403020. Some duplicates exist since their different attachments to the remaining part result in different molecular structures.

7 Details on the *in silico* hit-to-lead workflow

7.1 Used structure-based 3D molecular generative models

In this section, four state-of-the-art models are adopted that are designed to generate 3D molecules for a given protein pocket. Pocket2Mol[3] and DeepICL[4] are auto-regressive models with a distinctive generation mechanism. Pocket2Mol sequentially adds atoms and bonds to generate a 3D molecular graph within a protein pocket. DeepICL sequentially adds atoms, explicitly considering non-covalent interactions with surrounding protein atoms. TargetDiff[5] and DecompDiff[6] are diffusion models, where TargetDiff denoises atom positions and types with a 3D equivariant diffusion model, while DecompDiff decomposes each ligand into a scaffold and arms and uses specialized priors for sampling.

7.2 Target selection criteria and statistics of generated molecules

With these four models, we first generate 100 molecules, each for 100 protein pockets from the test set of the CrossDocked2020 dataset[7] following Luo et al. [8], which is a widely used benchmark for modern structure-based molecular generative models. After generation, we computed the QED and SA score of each generated molecule. Then, we selected targets with an average QED of generated molecules lower than 0.6, and an average SA greater than 3.5, leading to three targets with PDB ID 4P77, 4RV4, and 2EWY, respectively. We provide the statistics of the average QED and SA score of the molecules generated by each model in Table 5.

PDB ID	Model	QED (\uparrow)	SA (\downarrow)
4P77	DeepICL	0.44	3.63
	Pocket2Mol	0.52	3.58
	TargetDiff	0.35	4.21
	DecompDiff	0.57	3.70
4RV4	DeepICL	0.44	3.88
	Pocket2Mol	0.57	3.51
	TargetDiff	0.24	4.85
	DecompDiff	0.39	4.06
2EWY	DeepICL	0.55	4.14
	Pocket2Mol	0.41	4.92
	TargetDiff	0.33	5.64
	DecompDiff	0.20	5.83

Supplementary Table 5: A table summarizing the average QED and SA scores for four different generative models across three selected targets.

7.3 Additional results

In Table 6, we provide additional results for the targets that are not shown in the main text.

PDB ID	Model	Strategy	Success Rate			
			QED	SA	Docking	Joint
4P77	DeepICL	Random	0.79	0.44	0.76	0.27
		Frequency-based	0.82	0.56	0.85	0.38
		MMPA-based	0.81	0.52	0.85	0.36
		DeepBioisostere	0.80	0.63	0.83	0.44
	Pocket2Mol	Random	0.77	0.45	0.66	0.22
		Frequency-based	0.76	0.51	0.75	0.28
		MMPA-based	0.77	0.44	0.75	0.23
		DeepBioisostere	0.74	0.61	0.68	0.36
	TargetDiff	Random	0.63	0.62	0.65	0.30
		Frequency-based	0.69	0.66	0.73	0.33
		MMPA-based	0.64	0.57	0.68	0.22
		DeepBioisostere	0.83	0.75	0.74	0.49
DecompDiff	Random	0.25	0.30	0.58	0.05	
	Frequency-based	0.46	0.42	0.83	0.15	
	MMPA-based	0.43	0.40	0.87	0.16	
	DeepBioisostere	0.71	0.93	0.82	0.55	
2EWY	DeepICL	Random	0.15	0.10	0.95	0.01
		Frequency-based	0.24	0.20	0.98	0.05
		MMPA-based	0.48	0.15	0.95	0.06
		DeepBioisostere	0.58	0.79	0.90	0.45
	Pocket2Mol	Random	0.15	0.11	0.85	0.02
		Frequency-based	0.28	0.27	0.89	0.07
		MMPA-based	0.43	0.31	0.89	0.12
		DeepBioisostere	0.63	0.75	0.75	0.34
	TargetDiff	Random	0.13	0.30	0.93	0.05
		Frequency-based	0.24	0.44	0.95	0.10
		MMPA-based	0.30	0.36	0.95	0.10
		DeepBioisostere	0.73	0.87	0.92	0.63
DecompDiff	Random	0.11	0.28	0.94	0.04	
	Frequency-based	0.24	0.43	0.95	0.10	
	MMPA-based	0.32	0.37	0.96	0.13	
	DeepBioisostere	0.76	0.92	0.94	0.69	

Supplementary Table 6: Additional results for two targets in the CrossDocked2020 benchmark dataset (PDB ID: 2E6D and 4Z2G). The best success rates among replacement strategies are highlighted in bold.

References

- [1] Seonghwan Seo, Jaechang Lim, and Woo Youn Kim. “Molecular Generative Model via Retrosynthetically Prepared Chemical Building Block Assembly”. In: *Advanced Science* 10.8 (2023), p. 2206674.
- [2] Adam Paszke et al. “Pytorch: An Imperative Style, High-Performance Deep Learning Library”. In: *Advances in neural information processing systems* 32 (2019).
- [3] Xingang Peng et al. “Pocket2mol: Efficient molecular sampling based on 3d protein pockets”. In: *International Conference on Machine Learning*. PMLR. 2022, pp. 17644–17655.
- [4] Wonho Zhung, Hyeongwoo Kim, and Woo Youn Kim. “3D molecular generative framework for interaction-guided drug design”. In: *Nature Communications* 15.1 (2024), p. 2688.
- [5] Jiaqi Guan et al. “3D Equivariant Diffusion for Target-Aware Molecule Generation and Affinity Prediction”. In: *International Conference on Learning Representations*. 2023.
- [6] Jiaqi Guan et al. “DECOMPDIFF: diffusion models with decomposed priors for structure-based drug design”. In: *Proceedings of the 40th International Conference on Machine Learning*. 2023, pp. 11827–11846.
- [7] Paul G Francoeur et al. “Three-dimensional convolutional neural networks and a cross-docked data set for structure-based drug design”. In: *Journal of chemical information and modeling* 60.9 (2020), pp. 4200–4215.
- [8] Shitong Luo et al. “A 3D generative model for structure-based drug design”. In: *Advances in Neural Information Processing Systems* 34 (2021), pp. 6229–6239.